



# On component isolation of conceptual advanced reactors

August 2022

*Changing the World's Energy Future*

Efe G Kurt, Ayhan Irfanoglu, Samyog Shrestha, Arun Prakash



*INL is a U.S. Department of Energy National Laboratory operated by Battelle Energy Alliance, LLC*

#### **DISCLAIMER**

This information was prepared as an account of work sponsored by an agency of the U.S. Government. Neither the U.S. Government nor any agency thereof, nor any of their employees, makes any warranty, expressed or implied, or assumes any legal liability or responsibility for the accuracy, completeness, or usefulness, of any information, apparatus, product, or process disclosed, or represents that its use would not infringe privately owned rights. References herein to any specific commercial product, process, or service by trade name, trade mark, manufacturer, or otherwise, does not necessarily constitute or imply its endorsement, recommendation, or favoring by the U.S. Government or any agency thereof. The views and opinions of authors expressed herein do not necessarily state or reflect those of the U.S. Government or any agency thereof.

# **On component isolation of conceptual advanced reactors**

**Efe G Kurt, Ayhan Irfanoglu, Samyog Shrestha, Arun Prakash**

**August 2022**

**Idaho National Laboratory  
Idaho Falls, Idaho 83415**

**<http://www.inl.gov>**

**Prepared for the  
U.S. Department of Energy  
Under DOE Idaho Operations Office  
Contract DE-AC07-05ID14517**

# On component isolation of conceptual advanced reactors

Samyog Shrestha,<sup>\*,a</sup> Efe G. Kurt,<sup>b</sup> Arun Prakash,<sup>c</sup> and Ayhan Irfanoglu<sup>d</sup>

<sup>a</sup>*PhD Student, Lyles School of Civil Engineering,  
Purdue University, West Lafayette, IN*

<sup>b</sup>*Research Scientist,  
Idaho National Lab, Idaho Falls, ID*

<sup>c</sup>*Associate Professor, Lyles School of Civil Engineering,  
Purdue University, West Lafayette, IN*

<sup>d</sup>*Professor, Lyles School of Civil Engineering,  
Purdue University, West Lafayette, IN*

\*Email: [shresth3@purdue.edu](mailto:shresth3@purdue.edu)

Number of pages: 46

Number of tables: 10

Number of figures: 22



## Abstract

Implementation of component isolation in nuclear industry is challenging due to gaps in research and the lack of specific guidelines. In this study, parameters affecting component-level isolation of advanced reactor vessels are identified based on a representative numerical model with explicit consideration of nonlinear soil-structure interaction (SSI). The objective of this study is to evaluate the effectiveness of, and to identify potential limitations of using conventional friction pendulum and lead-rubber bearings to seismically isolate vessels. It is found that slender vessels or components are particularly vulnerable to rotational accelerations at the isolation interface, which are caused by rotation of the sub-structure and by excitation of higher modes in the horizontal direction of the seismically isolated system. Component isolation is found to be more effective for relatively stiffer vessels and at sites with stiff soil properties. Considering that conventional isolators are deficient in resisting axial tension, it is observed that the optimum location for supporting a component to achieve seismic isolation, is at a cross-sectional plane passing through the center of mass of the vessel. These findings are corroborated by numerous simulations of the response of seismically isolated reactor vessels at different nuclear sites subject to a variety of ground motions.

**Keywords** — component isolation, MASTODON, SAP2000, nuclear vessel

## I. INTRODUCTION

Seismically isolated nuclear power plants were first constructed in France and South Africa in 1983 and 1984, respectively [1]. Several nuclear power plant designs have been proposed with seismic isolators, e.g. 4S (Super Safe, Small and Simple) [2], IRIS (International Reactor Innovative and Secure) [3], S-PRISM (Power Reactor Innovative Small Module) [4], ALMR (Advanced Liquid Metal Reactor) [5]. Well-engineered implementation of seismic isolation can be beneficial in terms of safety and economy. Such benefits rely upon the ability of the isolation system to reduce lateral force demands on the isolated superstructure and site-independent standardization of the superstructure. Typical superstructures in nuclear power plants have fundamental periods in the order of 0.1 seconds [6, 7]. When isolators are installed between the superstructure and its foundation, the isolated system exhibits longer period, often 2 seconds or longer, in the fundamental mode of vibration. This period elongation causes an increased displacement demand mostly endured by the flexible isolators with absorption of energy. The frequency content of the seismic motion transmitted to the superstructure is also altered due to period elongation. Isolation reduces the lateral forces and distortions in the isolated stiff superstructure.

In the United States, low damping rubber, lead-rubber with single central core, and friction pendulum isolators are qualified for use in safety-related nuclear structures [6]. They are considered appropriate because their mechanical properties are stable over design lifetime in the temperature range of 40°F to 80°F and their behavior can be captured by numerical models. At higher temperatures upto 120°F, there is negligible change in stiffness and damping of elastomeric bearing whereas the coefficient of friction in general decreases with increase in ambient temperature [8].

Lead-rubber isolators are composed of alternating layers of natural rubber and steel shims with top and bottom steel flange plates and a central cylindrical lead core. Low damping rubber isolators are similar to lead-rubber isolators but without the lead core [9]. Friction pendulum isolators consist of spherical sliding surface, slider coated with low friction, temperature resistant and chemically inert material (such as PTFE) and housing plate. Depending on the number of sliding surfaces, friction pendulum isolators are categorized as single, double or triple pendulum. All these isolators have been time-tested by successful application in non-nuclear infrastructure such as bridges and buildings in the US and abroad [9–11]. Such proven track record increases confidence in the technology and allows for easier transition to use them in the nuclear industry.

NUREG/CR-7253 [6] provides technical guidelines on base isolation of nuclear structures. Nuclear power plant structures are designed to remain elastic for design basis earthquake (DBE) shaking but must ensure performance of safety-related functions even when subjected to more extreme ground motions. Those extreme ground motions represent beyond design basis (BDB) level of shaking and can be characterized by a 100,000 year return period, site-specific uniform hazard response spectra (UHS) [6, 12]. The design basis level of shaking corresponds to site-specific ground motion response spectra (GMRS) [6] which has a return period between 10,000 to 100,000 years as defined by NRC RG 1.208 [13].

Base isolation designs are emerging in the nuclear industry. But, base isolation is not always economical when nuclear facilities are constructed in regions of low to moderate seismic hazard. This is due to the trade-off between cost incurred to install the seismic isolation system and cost savings resulting from reduced demands in the seismically isolated structure [14]. Deeply-embedded reactor buildings are also unlikely to be base isolated [15] for excessive additional costs associated with site excavation and construction of a physical stop required to limit excessive isolator displacement during unforeseen events. In such cases, component isolation could be an approach to qualify typical reactor vessel designs irrespective of site hazard [16]. The economic feasibility of component isolation comes from the small size of the isolated superstructure which requires limited number of seismic isolators and allows ease of inspection and maintenance. Component isolation can be implemented without changing the configuration of the safety-critical component in a nuclear power plant by installing isolators directly at locations where such components are designed to be supported [15]. In this study, we focus on reactor vessels which are arguably the most important safety-critical components in a nuclear facility. A reactor vessel is a cylindrical steel container with a welded hemispherical bottom head and a removable hemispherical top head. It holds nuclear fuel that powers the reactor core in a nuclear power plant thus providing barrier against potential leakage of radioactive material to the environment.

In the nuclear industry, seismic isolation of safety-critical components, such as reactor vessels, is limited and lacks specific guidelines. Among few studies in the literature focusing on seismic isolation of nuclear components, a study by Ebisawa et al. [17] investigated the benefits of seismically isolating an emergency transformer of a nuclear power plant. Two types of isolators, namely, lead rubber bearing and ball bearing with coil spring were considered. The transformer was supported

by isolation devices at its base and the soil domain was represented by springs and dashpots. The response of the transformer was computed by direct integration using time-series of seismic motion and a lumped mass model. The study showed that seismic isolation of the transformer effectively reduces seismic demands with maximum acceleration in the transformer lowered to around  $1/10^{th}$  of that in the transformer without seismic isolation. It also concluded that the acceleration response of isolated transformer is not sensitive to shear wave velocity of soil except when it is below 150 m/s [18]. The analysis was validated by data from two sets of experiments on concrete test blocks (10 blocks each 1.6m x 1.6m x 0.2m stacked vertically) isolated by rubber bearings and ball bearings, one subjected to a real earthquake and the other subjected to simulated ground motions using a shake table.

Component-level isolation has received relatively more attention outside the nuclear industry. It has been applied to raised floors systems, sensitive equipment, fragile artifacts, statues in museums, columns of ancient temples and liquid storage tanks among others. Kircher et al. [19] installed elastomeric isolators at the base of a circuit breaker in the switchyard of A.D. Edmonston Pumping Plant, California and evaluated its seismic performance. Ambient and forced vibration tests were conducted to obtain modes of vibration including periods and corresponding damping ratios of the isolated circuit breaker. The fundamental period and damping ratio of the circuit breaker with and without seismic isolation were used to evaluate responses based on a reference 0.5g ground acceleration response spectra. Substantial reduction in peak acceleration by a factor of 4 to 5 was reported by the use of seismic isolators. It was concluded that the isolators provide better protection for circuit breakers from earthquakes.

The need for seismic protection of valuable and fragile artifacts spurred studies on their seismic isolation. Forcellini et al. [20] used finite element analysis to conduct numerical simulations of an isolation system consisting of a sliding top plate and a fixed bottom plate to protect the sculpture of David created by Michelangelo in the early 16<sup>th</sup> century. An estimated 55% reduction in maximum shear forces and the bending moments at the base of the model were reported. In another study, shake table tests were conducted on a marble statue at the J. Paul Getty Museum, Malibu, California [21]. The statue was seismically isolated by sliding bearings. The test, which was limited to shaking in the horizontal direction, demonstrated that acceleration response in the statue was reduced to 10% of the motion in the shake table. There have been several improvements

in the design of seismic isolators for the Getty Museum after these shake table tests. The Museum now uses a three-plate sliding bearing with guide-rails to protect valuable objects of art [22]. This assembly prohibits uplift through the mechanical capture of the linear guide blocks to the rails they travel on.

Isolating several objects together on a platform rather than individually can be more economical in some cases, for example, in data centers and clean room facilities with raised floor systems. Lambrou and Constantinou [23] performed shake table tests on a friction pendulum raised floor seismic isolation system supporting a generic computer cabinet. They reported 30% to 70% reduction in peak horizontal acceleration response on top of the isolated floor as compared to conventional floor without isolation. Under non-isolated conditions, the tested cabinet underwent rocking and developed accelerations that would interrupt functioning of the system. Rocking and uplift of the cabinet was also observed while using seismic isolators in some tests when the vertical motion in the shake table exceeded 1g. Hamidi and Naggar [24] numerically evaluated the performance of friction pendulum bearings in isolating a raised upper floor carrying a piece of equipment. The primary structure was assumed to have a fixed base. The performance of the system was evaluated in terms of sliding displacement at the isolation level and acceleration at the center of gravity of the equipment subject to different harmonic and lateral earthquake excitation at the base of the primary structure. They concluded that raised floor systems can be isolated effectively to protect important contents inside the building.

Component isolation has also been implemented in wine storage tanks following a history of earthquake induced economic losses in the wine industry. Auad and Almazan [25] studied the performance of a three-dimensional seismic isolation system in isolating a legged wine storage tank. Vertical rocking isolation (VRI) system based on ISO3D device was used. ISO3D is a vertically flexible and laterally stiff device that consists of an articulated frame, a system of springs and an energy dissipation system. Two tank sizes were considered: a 3  $m^3$  tank with 4 legs and a 30  $m^3$  tank with 6 legs. The fluid was modeled as a mass attached to the tank walls. From the time-history analysis, average reduction in axial loads and shear loads on the legs of the wine tank was obtained to be about 60% each. Reyes and Almazan [26] developed an improved version of ISO3D with higher mass capacity making it suitable for a larger structures. They evaluated the response of an isolated wine storage tank numerically considering the tank filled with wine as a

lumped mass. Horizontal force reduction ratios between 7.4 and 10.9 and vertical force reduction ratios between 2 and 3.8 were obtained in the tank by the use of the isolation system.

Studies on seismically isolated free standing objects have identified vulnerability on such objects due to rocking effects followed by overturning during an earthquake depending on the size and aspect ratio of the object [27]. To mitigate this phenomenon, Roussis and Constantinou [28] proposed XY-FP isolator which is capable of preventing uplift. In principle, XY-FP isolator resembles a conventional friction pendulum. It consists of two concave stainless steel beams placed on top of and orthogonal to each other. The upper beam can slide parallel and perpendicular to the lower beam axis. The configuration through which the two beams are interconnected permits tension to develop in the bearing and thus prevents uplift. Seismic isolators that prevent uplift have also been proposed by other techniques such as prestressing the bearing, use of uplift-restraining devices and use of opposing arms interlocking upon small uplift [29]. Although three-dimensional models of uplift preventing isolators exist, they are not as widely accepted as conventional friction pendulum and elastomeric bearings. The current study is limited to the application of conventional seismic isolators which are accepted for use in the nuclear industry.

The studies described above use seismic isolators at the base of the component being isolated. A unique aspect of component isolation of reactor vessels in the nuclear industry is the location of isolation interface. Reactor pressure vessels are usually designed to be supported at certain height rather than at their base. This poses new questions on the effectiveness of typical horizontal seismic isolators in reducing lateral forces in the vessel when supported at different heights along the vessel and what that optimal location of support is.

An important aspect to consider for nuclear structures is the interaction of the structure with the surrounding soil. Interaction of conventional base isolated structures with soil has been studied by several researchers using empirical spring-dashpot representations of the soil medium. Novak and Henderson [30] analytically investigated the influence of SSI and possible effects of foundation rocking on the modal properties and acceleration response of base isolated structures. They concluded that the effect of SSI on modal properties and seismic forces is small when the isolators are ten times or more flexible than the soil. They also found that rocking in the isolators reduces the natural frequencies of the structure. Tongaonkar and Jangid [31] evaluated the effect of SSI in the response of a seismically isolated bridge by modeling the soil medium by horizontal

and rotational springs and dashpots. They concluded that consideration of SSI results in enhanced safety and reduction in design costs, although displacements may be larger with the isolator than without. Haiyang et al. [32] conducted shake table tests of a steel frame structure (1 m wide and 2.1 m tall) seismically isolated by lead rubber bearings and supported on pile foundation over a laminar box filled with sand. They tested seismically isolated and non-isolated models supported on rigid foundation with and without sand (shear wave velocity,  $v_s$ , around 200 m/s). They reported that SSI effect weakens the isolation efficiency of the isolation layer and the story drifts of the isolated structure increase due to SSI when the peak ground acceleration (PGA) of the input motion exceeds 0.1g. Consideration of SSI is more critical when the isolated structure is founded on deep and soft soils because such soils amplify the motion at long periods which may result in intense, harmful demands on isolated structures with elongated periods. The problem of long period ground motion is not just related to site amplification. There are numerous recorded ground motions with high energy in long periods not necessarily resulting from soil amplification. Thus, investigating the effect of SSI on nuclear structures, with and without seismic isolators, across a variety of soil conditions is of utmost importance.

The objective of this study is to investigate the seismic behavior of reactor vessels with conventional friction pendulum and lead-rubber isolators with the consideration of nonlinear soil-structure interaction. In this study, key parameters affecting the response of seismically isolated conceptual reactor vessels are identified based on information in existing literature [33]. Based on the containment structure layout of the ARC-100 nuclear reactor [34], several 3-dimensional models of conceptual reactor vessels, both with and without isolators, are constructed in MASTODON [35] (an open-source 3-dimensional finite element code) and SAP 2000 [36] (a commercially available finite element program). Several numerical simulations are conducted to assess the behavior of these reactor vessels when the chosen key parameters are varied across their respective ranges of interest. In these simulations, input ground motion is specified with all three components ( $x, y$  and  $z$ ) simultaneously at the base of the models, and nonlinear behavior of soil and seismic isolators is also considered. Possible causes for uplift of bearings and subsequent impact loading upon re-engagement are identified. SSI is considered by explicitly modeling soil profiles from real nuclear sites in these conceptual models representing different configurations of component-level isolation of reactor vessels.

## II. RESPONSE OF SEISMICALLY ISOLATED COMPONENTS

Figure 1 depicts a simplified model of a seismically isolated component - a nuclear vessel, for example. The vessel is held together by annular collar plates around its circumference which rest on top of seismic isolators. The isolators are supported by a foundation sub-structure which rests on the soil domain, represented here as translational and rotational springs. The component has an overall height  $H$  and is supported at a height  $\phi H$  from its base. This model will be used to identify parameters that influence the acceleration response of seismically isolated components and the axial forces that develop in the isolators.

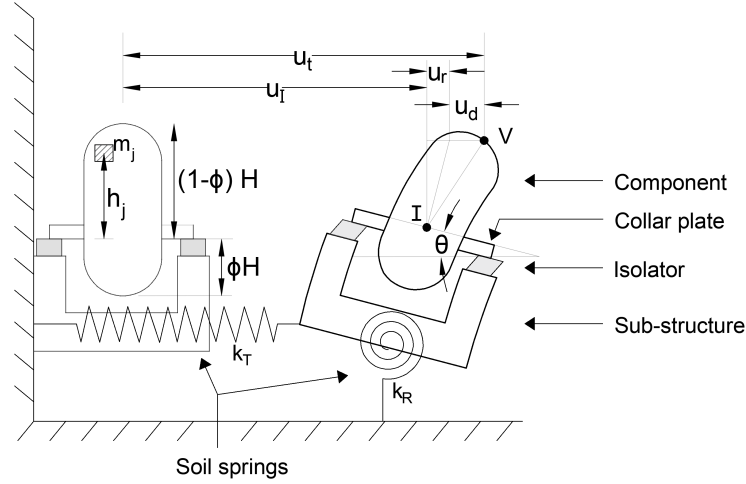


Fig. 1. Schematic figure of a conceptual component isolation model

Shown in the figure is an arbitrary displaced configuration of the model at any instant during the seismic excitation. We define the surface of contact between the collar plate and the isolators as the isolation interface. Let point I be the geometric centroid of the isolation interface and point V be the top-most point of the component. The total horizontal displacement of the top of the component,  $u_t$  can then be expressed as:

$$\begin{aligned} u_t &= u_I + u_r + u_d \\ &= u_I + \theta (1 - \phi) H + u_d \end{aligned}$$

where,  $u_I$  is the horizontal displacement of point I,  $u_r$  and  $u_d$  are horizontal displacements resulting from rotation at the isolation interface and deformation in the component respectively,  $\theta$  is the



(small angle) rotation at the isolation interface.

The acceleration at the top of the component can thus be expressed as:

$$\ddot{u}_t = \ddot{u}_I + \ddot{\theta} (1 - \phi) H + \ddot{u}_d \quad (1)$$

where,  $\ddot{u}_I$  and  $\ddot{\theta}$  are the horizontal and rotational accelerations, respectively at the isolation interface and  $\ddot{u}_d$  is the horizontal acceleration due to deformations in the vessel. These accelerations are time-dependent and peak acceleration in the vessel depends on a combination of the terms on the right hand side of Eq. 1.

Figure 1 shows an infinitesimal element of the component with mass  $m_j$ , located at height  $h_j$  from the support (i.e. the isolation interface), and undergoing a horizontal acceleration  $\ddot{u}_j$ . The moment about point I  $M_I$ , due to inertial forces on all such elements in the vessel, can be expressed as:

$$\begin{aligned} M_I &= \sum m_j \ddot{u}_j h_j \\ &= \sum m_j \left[ \ddot{u}_I + \ddot{\theta} h_j + (\ddot{u}_d)_j \right] h_j \end{aligned}$$

This moment leads to imbalance in the axial forces of the isolators which can cause undesirable tensile forces and uplift in the isolators. In extreme cases, it can lead to overturning of the vessel itself. The expression for this overturning moment can further be expanded as:

$$\Rightarrow M_I = \ddot{u}_I \sum m_j h_j + \ddot{\theta} \sum m_j h_j^2 + \sum m_j h_j (\ddot{u}_d)_j \quad (2)$$

To avoid uplift in the isolators, the overturning moment about the isolation interface  $M_I$  should be minimized during a seismic event. While it is possible that the three terms in the expression for  $M_I$  in Eq. 2 cancel each other out, the other extreme, when the three terms collude to maximize  $M_I$ , is worth paying attention to. This would happen, when the components of the horizontal acceleration listed in Eq. 1 contribute to inertial forces in the same direction. For example, when the isolation interface is accelerating to the right, the rotational acceleration is clockwise, and acceleration due to deformation is also to the right (which would be the case for deformation in the first mode), then the effect of the three terms in Eq. 2 is maximized. Consequently, to

minimize  $M_I$  under such a scenario, each term in Eq. 2 must be minimized. The first term in Eq. 2 can be eliminated by supporting the vessel such that the isolation interface passes through its center of mass. The second term depends upon rotational acceleration at the isolation interface and mass moment of inertia of the vessel ( $\sum m_j h_j^2$ ) about its isolation interface. This term is also minimized by ensuring that the isolation interface passes through the center of mass of the vessel. Finally, the third term is minimized by minimizing deformations in the vessel. Since deformation of the vessel depends upon the ground motion as well as the modal frequency of the vessel, this can be achieved by designing the vessel to be stiff compared to the expected frequency content of the ground motion.

The analytical model shown in Figure 1 indicates that key parameters that influence the acceleration response of the seismically isolated vessel and the axial forces that develop in the isolators are the fundamental frequency of the vessel, relative location of isolators ( $\phi$ ) supporting the vessel, and stiffness properties of soil and isolators. Next, we study the behavior of isolated components as these key parameters are varied.

### III. REACTOR VESSELS IN THE NUCLEAR INDUSTRY

The International Atomic Energy Agency (IAEA), an independent global organization focused in ensuring safe and peaceful use of nuclear energy, maintains a web-accessible database [33] titled 'Advanced Reactors Information System (ARIS)' which contains up-to-date information about 50 existing and proposed advanced reactor designs. Figure 2 presents technical data in the form of histogram representing total number of advanced reactors that have a certain range of physical properties such as wall thickness, height, transport weight and aspect ratio (ratio of height to diameter). The properties of reactor vessels chosen in this study are also marked in the figure. Parameters chosen for vessels in this study make them relatively tall and slender in comparison to existing vessels, because such vessels are more vulnerable to higher seismic demand. We do not consider variations in wall thickness of the vessels because it does not noticeably affect the fundamental frequency of typical vessels with thin walls.

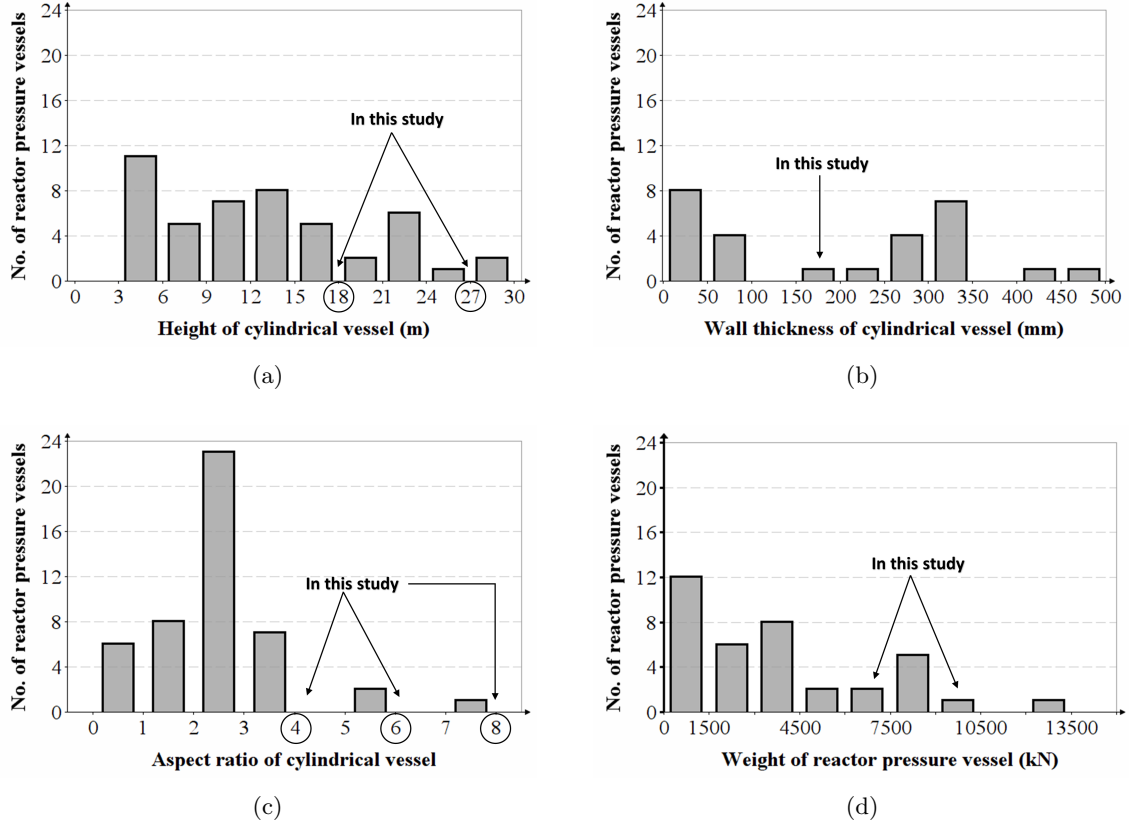


Fig. 2. Properties of existing and proposed reactor pressure vessels. (Note: The histograms are created using data published by IAEA [33])

#### IV. MODELING APPROACH

A typical 3-dimensional model of a nuclear vessel resting on isolators on top of a foundation substructure supported by a soil domain is shown in Figure 3. The reactor vessel and its collar plate are both modeled using beam elements. The reactor vessel is seismically isolated using four isolators that are supported atop a sub-structure that forms a reactor silo (7.9m x 7.9m in the horizontal plane and 11m deep embedded in soil) and the foundation mat (24.4m x 24.4m x 1.2m). Layout of this sub-structure and size of the foundation are based on the design of ARC-100 reactor [34]. It is assumed that the geometry of the silo does not appreciably impact the response of the vessel. So, to simplify the numerical model, a prismatic shape similar to that proposed by Kammerer et al. [15] is considered in this study. The sub-structure is modeled by solid elements with linear elastic material and the soil domain is modeled by solid elements with

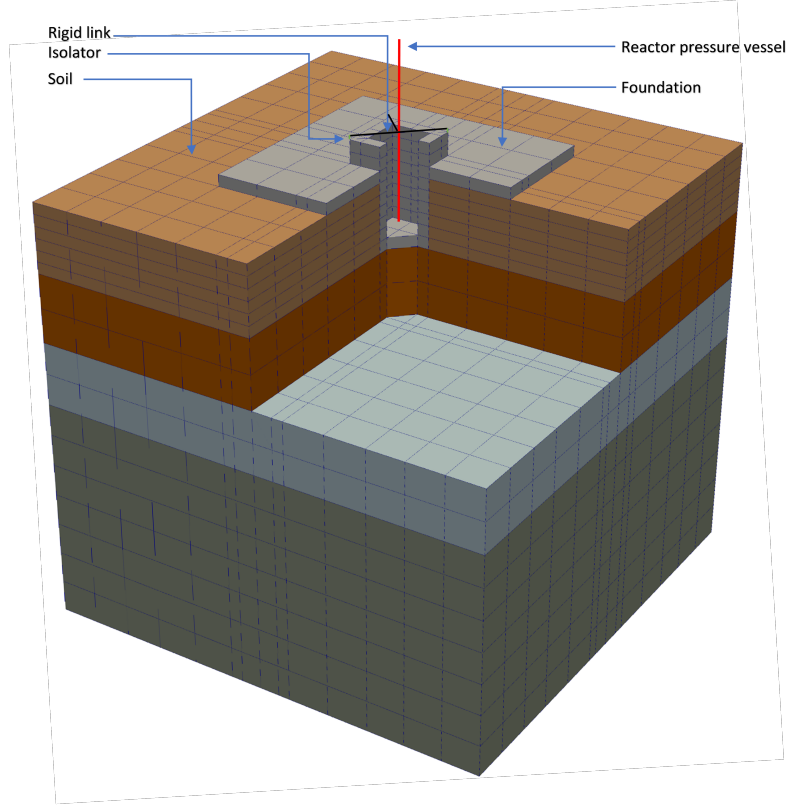


Fig. 3. Cutaway view of component isolation model.

nonlinear hysteretic material described in detail in the next section.

Width of soil domain is taken as 48.8m which is sufficiently wide to avoid spurious reflections from the artificial boundary of the soil-model. Periodic boundary conditions are imposed on opposite vertical faces of the soil domain by constraining them to move identically at each elevation. Rock outcrop motions are applied at the transmitting (non-reflecting) base of the soil domain as shear and normal traction inputs. The 3-component traction time series, i.e. along two horizontal (X- and Y-) and one vertical (Z-) direction, are computed as:

$$\tau_X(t) = \rho^{br} v_s^{br} v_X(t) \quad (3)$$

$$\tau_Y(t) = \rho^{br} v_s^{br} v_Y(t) \quad (4)$$

$$\sigma(t) = \rho^{br} v_p^{br} v_Z(t) \quad (5)$$

where,  $\rho^{br}$ ,  $v_s^{br}$ ,  $v_p^{br}$  are, respectively, the density, s-wave velocity, and p-wave velocity of the underlying bedrock. Shear traction time series along X- and Y- directions are denoted  $\tau_X(t)$  and  $\tau_Y(t)$  respectively and  $\sigma(t)$  is the normal traction time series. The velocity time series of the rock outcrop motion along X-, Y- and Z- directions is denoted as  $v_X(t)$ ,  $v_Y(t)$  and  $v_Z(t)$  respectively. For hard rock sites, the soil domain is idealized as a fixed base in accordance with ASCE 4-16 [37] recommendations by introducing a Dirichlet boundary condition at the base of the isolators. In such fixed base models, rock outcrop accelerations are directly prescribed at the base.

### Choice of Numerical Parameters

Element size for the soil domain is computed using Eq. 6 as per recommendations by Kuhlemeyer and Lysmer [38].

$$\Delta z = \frac{v_s}{10f_{max}} \quad (6)$$

This is equivalent to discretizing the harmonic wave at one-tenth of the shortest period seismic wave that can be transmitted accurately in the model [39]. The shortest wave period considered is 0.04 seconds, corresponding to maximum considered frequency of 25 Hz which is greater than the fundamental frequency of the vessels considered in this study.

Element size for beam elements is selected such that its fundamental frequency does not change on further refinement of mesh. The vertical beam that represents the vessel is discretized into 30 elements whereas the link beams representing the collar plates are discretized into 8 elements each.

Analysis is carried out using a time-step of 0.005s. Dynamic response is computed using Hilber-Hughes-Taylor (HHT)- $\alpha$  integration scheme ( $\alpha = -0.3$ ,  $\beta = 0.4225$  and  $\gamma = 0.8$ ) [40].

## V. MATERIAL PROPERTIES AND MATERIAL MODELS

### Reactor pressure vessels and substructure

For numerical analysis, we study the response of four models of a reactor pressure vessel (RPV) listed in Table I. We also investigated RPV models supported at three quarter height from its bottom (i.e.  $\phi = 0.75$ ) and found that the fundamental frequency and peak acceleration are

identical to cases with  $\phi = 0.25$ . Such models are therefore not listed in the table. Similarly, RPV model ID - III and IV supported at mid-height are not considered to be critical because they are less likely to undergo rocking or have uplift in the isolators compared to models with  $\phi = 0.25$  and are thus omitted from the table.

The reactor vessel is considered to be a cylindrical vessel made of steel with uniform wall thickness and mass distribution. A 3D shell-element model and its equivalent beam-element model is shown in Figure 4. The mass of the internal contents, for example, controls rods, reactor core, pumps, reactor cooling system, etc., are added to the mass of the cylindrical vessel and assumed to have no contribution on the stiffness of the vessel. The mass of the internal contents is taken as 50% of the total mass of vessel. This assumption is made due to insufficient publicly available information on the actual distribution of mass within typical RPVs. In the beam-element model, the collar plates are replaced with ‘link beams’ that transfer the weight of the vessel to the isolators. Flexural rigidity ( $EI$ ) of these link beams is taken such that the beam-element model captures the first four modes of the shell-element model having 18-inch thick collar plate. It results in a value of  $EI$  for each of the four link beams that is equal to that of the vessel. Linear-elastic material properties are used for steel (in the RPV) and concrete (in the sub-structure) with values taken from ASCE 4-16 [37] and tabulated in Table II.

TABLE I  
Description of RPV models

| SN | Model ID | Vessel height, H (m) | Aspect ratio, $\lambda$ | Vessel weight (kN) | Support location, $\phi$ | Fundamental freq. (Hz) |
|----|----------|----------------------|-------------------------|--------------------|--------------------------|------------------------|
| 1  | I        | 18.3                 | 4                       | 7260               | 0.5                      | 23.8                   |
| 2  | II       | 18.3                 | 4                       | 7260               | 0.25                     | 13.1                   |
| 3  | III      | 27.4                 | 6                       | 10890              | 0.25                     | 6.3                    |
| 4  | IV       | 27.4                 | 8                       | 10075              | 0.25                     | 4.9                    |

TABLE II  
Material properties

| SN | Material | Elastic modulus (GPa) | Poisson’s ratio | Unit weight ( $kN/m^3$ ) |
|----|----------|-----------------------|-----------------|--------------------------|
| 1  | Concrete | 27.6                  | 0.17            | 23.6                     |
| 2  | Steel    | 200                   | 0.3             | 78.5                     |

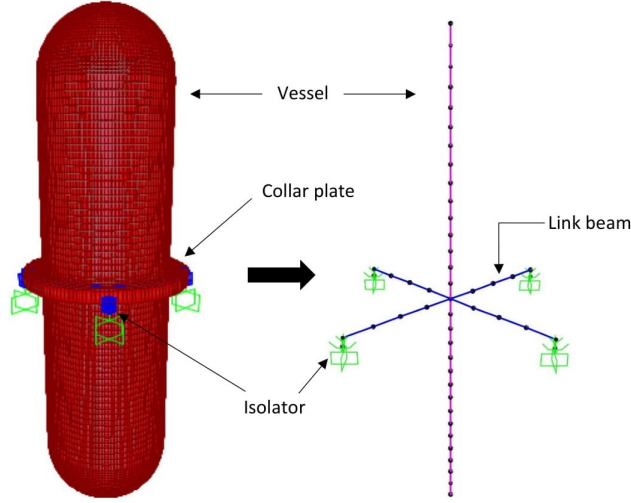


Fig. 4. A 3D shell-element model of a reactor pressure vessel with collar plates and its equivalent beam-element model.

### Seismic isolators

In this study, single friction pendulum isolators are first designed using an equivalent static approach (for detailed explanation, see Kelly and Naiem [9] and AASHTO GSID [41]). For the design, the sub-structure supporting the isolators and the component supported by the isolators are assumed to be rigid to ensure a uniform design of the isolator used in different models analyzed. The properties of single friction pendulum isolator for different cases are tabulated in Table III. For reference, properties of a lead-rubber isolator that resembles the effective period and damping of this single friction pendulum bearing are also listed in Table IV.

The isolator design procedure is briefly summarized in the following steps:

1. Determine yield force ( $Q$ ) of the isolator using assumed constant friction coefficient ( $\mu$ ) and known total weight of the component ( $W$ ):  $Q = \mu W$
2. Assume a design displacement ( $\Delta$ ) of the isolators.
3. Determine post-yield stiffness ( $k_1$ ):  $k_1 = 0.05 \frac{W}{\Delta}$

4. Determine effective stiffness ( $k_{eff}$ ) and period ( $T_{eff}$ ) of the isolator:

$$k_{eff} = \frac{Q + k_1 \Delta}{\Delta}$$

$$T_{eff} = 2\pi \sqrt{\frac{W/g}{k_{eff}}}$$

5. Determine equivalent damping ratio ( $\xi$ ) and damping coefficient ( $B_L$ ) of the isolator:

$$\xi = \frac{4 Q \Delta}{2\pi k_{eff} \Delta^2}$$

$$B_L = \begin{cases} \left(\frac{\xi}{0.05}\right)^{0.03} & \text{if } \xi \leq 0.3 \\ 1.7 & \text{if } \xi > 0.3 \end{cases}$$

6. Determine displacement of bearing and iterate until its convergence.

$$\Delta = \frac{T_{eff}}{4\pi^2} \frac{S_{D1} g}{B_L}$$

where,  $S_{D1}$  is design spectral acceleration at 1-second period normalized by acceleration due to gravity ( $g$ ). It is taken greater than the design level shaking of all sites considered in this study to ensure that the bearings do not exceed their design displacement, a value of 0.4 is used.

7. Determine effective radius of curvature ( $R_{eff}$ ) of concave sliding surface:  $R_{eff} = \frac{W}{k_1}$
8. Determine final design displacement ( $\Delta_f$ ) for bi-directional shaking considering 100% design displacement in one direction and 30% in another direction:  $\Delta_f = 1.3 \Delta$

TABLE III  
Properties of single friction pendulum isolator

| SN | RPV model ID | Friction coeff. $\mu$ | Weight on each isolator (kN) | Radius of curvature (m) | Effective period (s) | Design disp. (cm) | Stiffness (kN/mm) |            |
|----|--------------|-----------------------|------------------------------|-------------------------|----------------------|-------------------|-------------------|------------|
|    |              |                       |                              |                         |                      |                   | Initial           | Post-yield |
| 1  | I / II       | 0.06                  | 1815                         | 2.5                     | 2.1                  | 15                | 108               | 0.7        |
| 2  | III          |                       | 2720                         |                         |                      |                   | 162               | 1.1        |
| 3  | IV           |                       | 2015                         |                         |                      |                   | 120               | 0.8        |



TABLE IV  
Properties of lead-rubber isolator

| SN | RPV<br>model<br>ID | $t_r$<br>(mm) | $t_s$<br>(mm) | n  | $D_1$<br>(mm) | $D_2$<br>(mm) | $f_y$<br>(kN) | $\alpha$ | Stiffness (kN/mm) |                     |            |
|----|--------------------|---------------|---------------|----|---------------|---------------|---------------|----------|-------------------|---------------------|------------|
|    |                    |               |               |    |               |               |               |          | Axial             | Shear<br>post-yield | Rotational |
| 1  | I                  | 6             | 3             | 20 | 125           | 500           | 110           | 0.0381   | 802.7             | 0.7                 | 51.1       |

$t_r$  = Thickness of rubber layer,  $t_s$  = Thickness of steel shims,  $n$  = No. of rubber layers  
 $D_1$  = Diameter of lead plug,  $D_2$  = Diameter of bearing  
 $f_y$  = Yield force,  $\alpha$  = Post-yield to elastic shear stiffness ratio

### Single friction pendulum isolator model

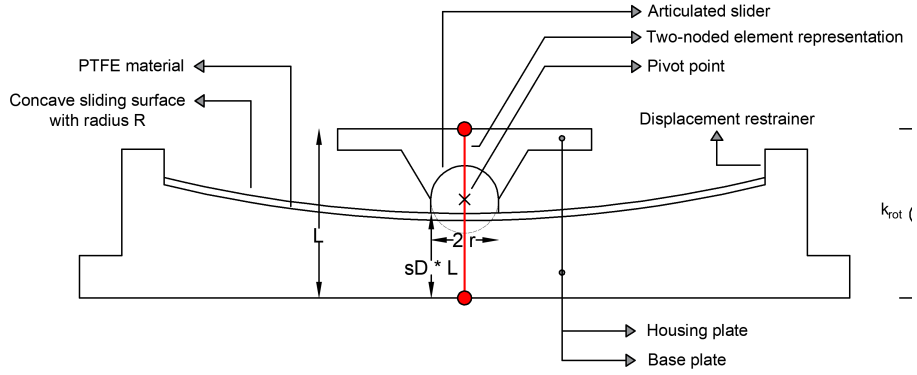


Fig. 5. Model of a typical single concave friction pendulum

A two-noded beam element model developed by Kumar et al. [42] is implemented in MASTODON. Figure 5 shows a typical single friction pendulum isolator as first proposed by Zayas et al. [43] and its two-noded element representation. In the isolator model, the single element extends from the bottom of the base plate to the top of the housing plate. Distance from the bottom node of the isolator to the sliding surface as a ratio of the element length ( $L$ ) is termed as shear-distance ratio ( $sD$ ). Throughout this study, we use a value of 0.5 for the shear-distance ratio. The isolator element has 6 degrees of freedom - axial, two shear, two rotational and torsional.

An ideal force-displacement relationship for shear degrees of freedom is presented in Figure 6. The shear stiffness of the isolator before sliding is given by:

$$k_0 = \frac{Q}{u_y}$$

where,  $Q$  is the yield force and  $u_y$  is the yield displacement of the isolator. After exceedence of

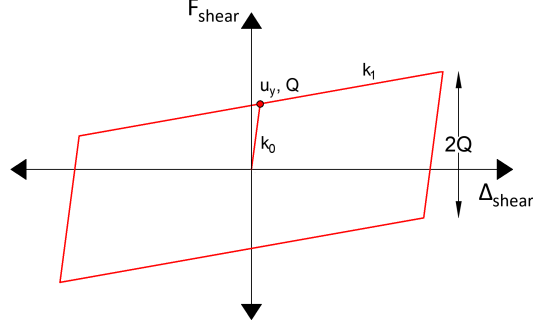


Fig. 6. Force displacement relationship for single friction pendulum isolator

frictional resistance, it exhibits relatively smaller stiffness given by:

$$k_1 = \frac{W}{\sqrt{R_{eff}^2 - u^2}}$$

The material models in both MASTODON and SAP2000 are based on two-noded single element exhibiting coupled friction properties for the two shear deformations and linear stiffness properties for axial and moment deformations. Models have gap behavior in axial tension. The material model in SAP2000 is based on Wen [44] and Park, Wen and Ang [45] in contrast to bilinear plasticity formulation in MASTODON. For consistency between the two analysis codes, the factors accounting for the effect of sliding velocity, contact pressure and temperature on the coefficient of friction are set to unity to model constant friction coefficient throughout analysis.

### Lead-rubber isolator model

Lead-rubber (LR) bearings are composed of alternating layers of natural rubber and steel shims with top and bottom steel flange plates and a central cylindrical lead core. MASTODON adopts a two-noded isolator element model developed by Kumar et al. [46], which is capable of simulating nonlinear behavior in axial (including buckling and cavitation) and shear directions. Smoothed hysteretic behavior proposed by Park et al. [45] and extended by Nagarajaiah et al. [47] is used to model the behavior of a lead-rubber bearing in shear in both MASTODON and SAP2000. The isolator model in SAP 2000 is linear elastic in axial direction and does not capture buckling and cavitation.

## Soil Profiles

Six soil profiles from operating nuclear power plants in the U.S. representing hard rock, stiff soil and soft soil sites are selected. The classification of site is based on NEHRP Provisions [48]. Table V summarizes the shear wave velocity of top 30m layer of soil ( $v_{s30}$ ) and the total soil depth for those sites. Shear wave velocity of 2830 m/s and Poisson's ratio of 0.25 are adopted for bedrock of all sites. Shear wave velocity profile of the sites are presented in Figure 7.

TABLE V  
Summary of soil profiles for this study

| SN | Station name      | State | $v_{s30}$<br>(m/s) | Depth<br>(m) | GMRS     |          | UHRs ( $10^{-5}/\text{yr}$ ) |          |
|----|-------------------|-------|--------------------|--------------|----------|----------|------------------------------|----------|
|    |                   |       |                    |              | $S_{DS}$ | $S_{D1}$ | $S_{DS}$                     | $S_{D1}$ |
| 1  | Oconee            | SC    | 2520               | 20.4         | 0.40     | 0.08     | 0.80                         | 0.15     |
| 2  | Byron             | IL    | 975                | 36.6         | 0.27     | 0.07     | 0.58                         | 0.14     |
| 3  | Pilgrim           | MA    | 875                | 42.7         | 0.51     | 0.06     | 1.06                         | 0.13     |
| 4  | Monticello        | MN    | 457                | 33.5         | 0.15     | 0.04     | 0.33                         | 0.07     |
| 5  | H.B.Robinson      | SC    | 390                | 140.2        | 0.47     | 0.31     | 0.92                         | 0.64     |
| 6  | Palisades Nuclear | MI    | 305                | 45.1         | 0.30     | 0.15     | 0.60                         | 0.30     |

GMRS = Ground motion response spectrum, UHRs = Uniform hazard response spectrum

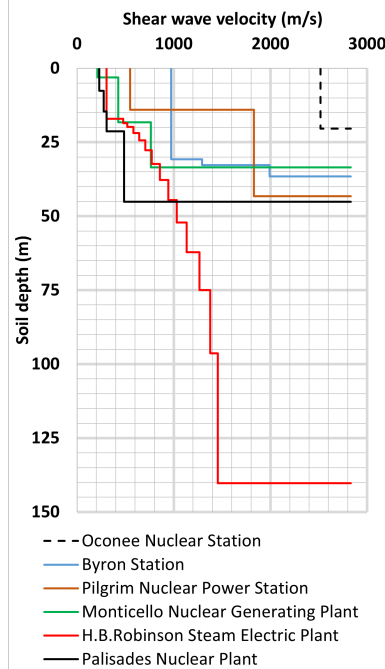


Fig. 7. Shear wave velocity profiles from selected sites

Site hazard data are available for all sites [49–54] in terms of uniform hazard response spec-

trum (UHRS) with a return period of 100,000 years representing a beyond design level event and ground motion response spectrum (GMRS) which represents a design level event as per NUREG/CR-7253 [6]. The spectral acceleration parameters  $S_{DS}$  and  $S_{D1}$  are presented in Table V. These parameters  $S_{DS}$  and  $S_{D1}$  are respectively obtained by normalizing the 5% damped response spectral acceleration at short period (0.01s) and 1-second period by acceleration due to gravity. The design level response spectra for the sites are presented in Figure 8 along with a reference acceleration spectrum of the ground motion during the 1989 Loma Prieta earthquake obtained at Gilroy-1 station [55].

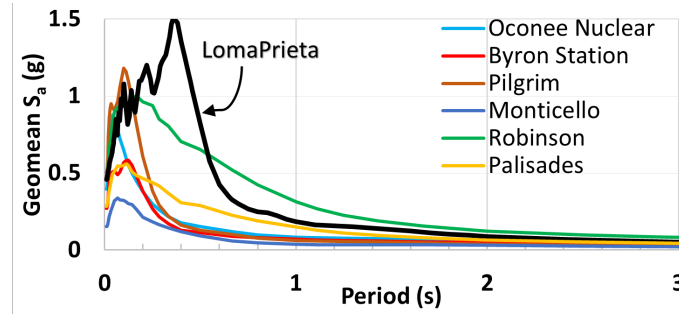


Fig. 8. Design level response spectra of sites considered in this study

### Soil model

The *I-soil* material model in MASTODON is used in this study. The model is represented as nested spring and slider components with different stiffness values in one dimensional shear stress space [35]. Its framework is analogous to the distributed element modeling concept developed by Iwan [56]. The model behavior is obtained by superimposing the stress-strain response of those nested components [57]

Three-dimensional generalization of the soil model follows Chiang and Beck [58] using von Mises yield criterion and an associative flow rule. Nonlinear hysteretic behavior of soil is achieved by defining piecewise linearized backbone curve. Backbone curves are generated as:

$$\tau^i(\gamma) = G/G_{max}^i(\gamma) * G_{max}^i * \gamma \quad (7)$$

where  $\tau^i(\gamma)$  and  $G/G_{max}^i(\gamma)$  are both functions of shear strain  $\gamma$  and represent the shear stress and modulus reduction of the  $i^{th}$  soil layer. EPRI (1993) [59] and Vucetic and Dobry (1991) [60]

modulus reduction curves are used for rock (or sand) and clay respectively. The soil model uses Masing rule for hysteretic reloading / unloading.

## VI. INPUT MOTION

Five ground motions (all 3-components) recorded at rock outcrop are selected such that they cover a wide range of peak ground acceleration (PGA) from 0.2g to 0.9g. The short-period spectral acceleration parameter ( $S_{DS}$ ) for the selected sites also fall within that range. The PGA in two horizontal directions is combined by geometric mean. The ground motion data are obtained from PEER database [55] enforcing a lower limit criteria on magnitude of earthquake as 6 and shear wave velocity of site where motion was recorded as 700 m/s to include only rock-outcrop motions. These ground motions are listed in Table VI.

TABLE VI  
Summary of ground motions

| SN | Earthquake      | Station   | Year of earthquake | $M_w$ | PGA (g) | PGV (cm/s) | $S_{D1}$ | Peak vertical acc. (g) |
|----|-----------------|-----------|--------------------|-------|---------|------------|----------|------------------------|
| 1  | Kocaeli, Turkey | Izmit     | 1999               | 7.5   | 0.20    | 30.5       | 0.28     | 0.12                   |
| 2  | Hector Mine     | Hector    | 1999               | 6.9   | 0.30    | 33.5       | 0.32     | 0.15                   |
| 3  | Loma Prieta     | Gilroy-1  | 1989               | 6.9   | 0.46    | 33.5       | 0.19     | 0.21                   |
| 4  | Manjil, Iran    | Abbar     | 1990               | 7.4   | 0.51    | 45.7       | 0.44     | 0.48                   |
| 5  | Duzce, Turkey   | IRIGM 496 | 1999               | 7.1   | 0.89    | 39.6       | 0.23     | 0.32                   |

$M_w$  = Moment magnitude

The acceleration time-series of ground motions considered for this study are presented in Figure 9. For each ground motion, 3-components are plot as East-West (EW), North-South (NS) and Up-Down (UD). The spectral accelerations (5 % damped) for individual ground motion are shown in Figure 10.

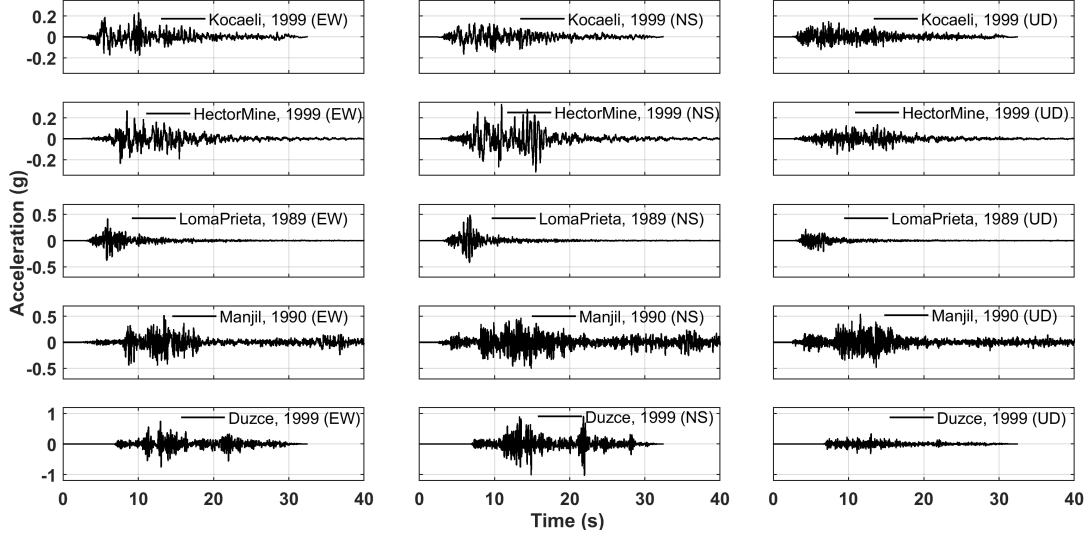


Fig. 9. Acceleration time-series of ground motions selected for this study

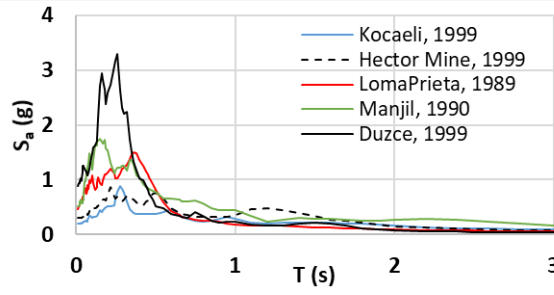


Fig. 10. Acceleration response spectra of ground motions selected for this study

## VII. RESULTS

To present the results of the time-history analyses in a representative manner, the following metrics are defined. The peak horizontal acceleration in the vessel is defined as the geometric mean (geomean) of the peak acceleration in the East-West and North-South directions, expressed as:

$$a_{peak} = \sqrt{\ddot{x}_{max} \ddot{y}_{max}} \quad (8)$$

where,  $\ddot{x}_{max}$  and  $\ddot{y}_{max}$  are the peak East-West (EW) and North-South (NS) component accelerations. Reduction in peak horizontal acceleration of the reactor vessel ( $a_{peak}$ ) due to seismic

isolation is defined as:

$$\eta_a = \left[ 1 - \frac{(a_{peak})_{iso}}{(a_{peak})_{non-iso}} \right] \times 100\% \quad (9)$$

where,  $(a_{peak})_{iso}$  and  $(a_{peak})_{non-iso}$  are the peak horizontal accelerations (geomean) for the isolated and non-isolated case.

Axial forces in an isolator deviate from the static load due to vertical acceleration and overturning moment ( $M_I$ ) developed at the isolation interface. The minimum axial compression in the four isolators during the entire seismic event is denoted as  $P_{min}$ .

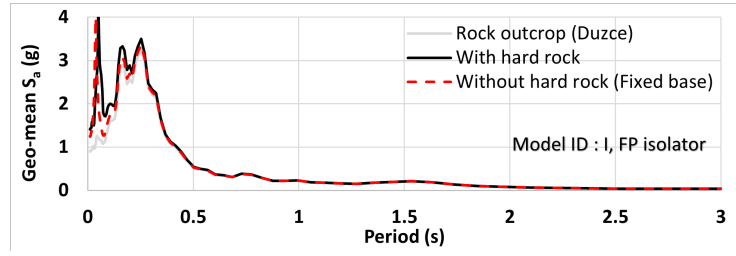
### Observations from analyses conducted for hard rock sites

It is observed that for hard rock sites, the rotation at the isolation interface is negligible and peak accelerations in the vessel can be approximated from a fixed base analysis where the bottom nodes of the four isolators are subjected to 3-component rock-outcrop accelerations. Such a comparison is presented in Figure 11. The plot compares spectral acceleration at the top of the vessel from two analyses with RPV Model ID - I. In one analysis, the hard rock site is modeled as shown in Figure 3 and in the other analysis, the hard rock site is replaced by fixed base (i.e. with no substructure and no soil). The input motion used for this comparison is Duzce, 1999 which has a PGA of 0.89g.

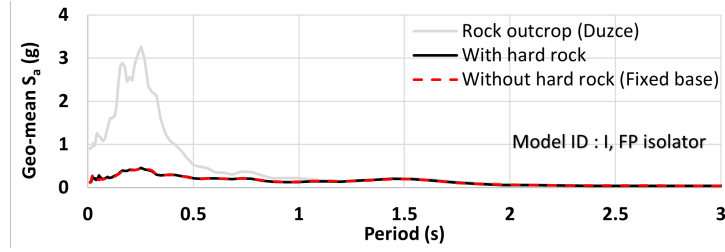
### Comparison of result between SAP 2000 and MASTODON

Results from numerical analysis in MASTODON are compared against those from SAP 2000 using a fixed base model which is representative of hard rock condition. Both SAP 2000 and MASTODON produce identical results with small discrepancies attributable to differences in the material models. Some of the analysis results are presented in Figure 12. The analysis corresponds to RPV Model ID - I with friction pendulum isolators subjected to 3-component input motion from Loma Prieta earthquake. The force-displacement relationship along East-West and North-South direction are compared in Figure 12(a) and 12(b) respectively. Figure 12(c) compares the 5% damped spectral acceleration at the top of the vessel using geometric mean to combine the response in East-West and North-South directions.

Similar analyses are also conducted with lead-rubber bearing isolators in MASTODON and

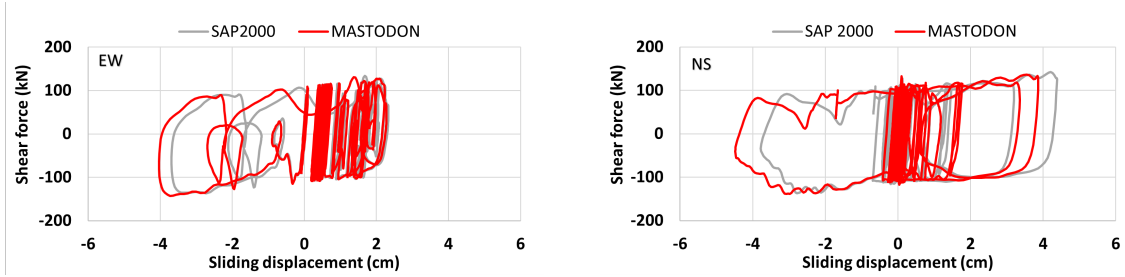


(a) Non-isolated



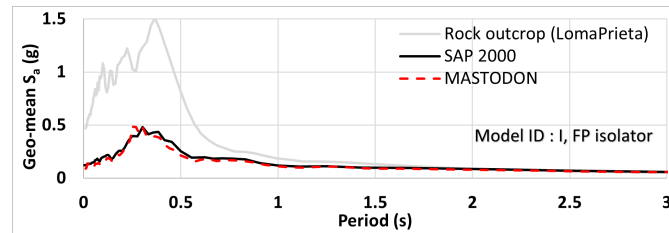
(b) Isolated

Fig. 11. Comparison of response in isolated (friction pendulum) vessel for model ID - I



(a) Force-displacement plot (East-West)

(b) Force-displacement plot (North-South)



(c) 5% damped spectral acceleration

Fig. 12. Comparison of response in isolated (friction pendulum) vessel for fixed base model ID - I

SAP 2000. The analysis results in Figure 13 are for RPV corresponding to Model ID - I with lead-rubber isolators subjected to base excitation by Loma Prieta ground motion. The force-displacement relationship along East-West and North-South directions are compared in Figures



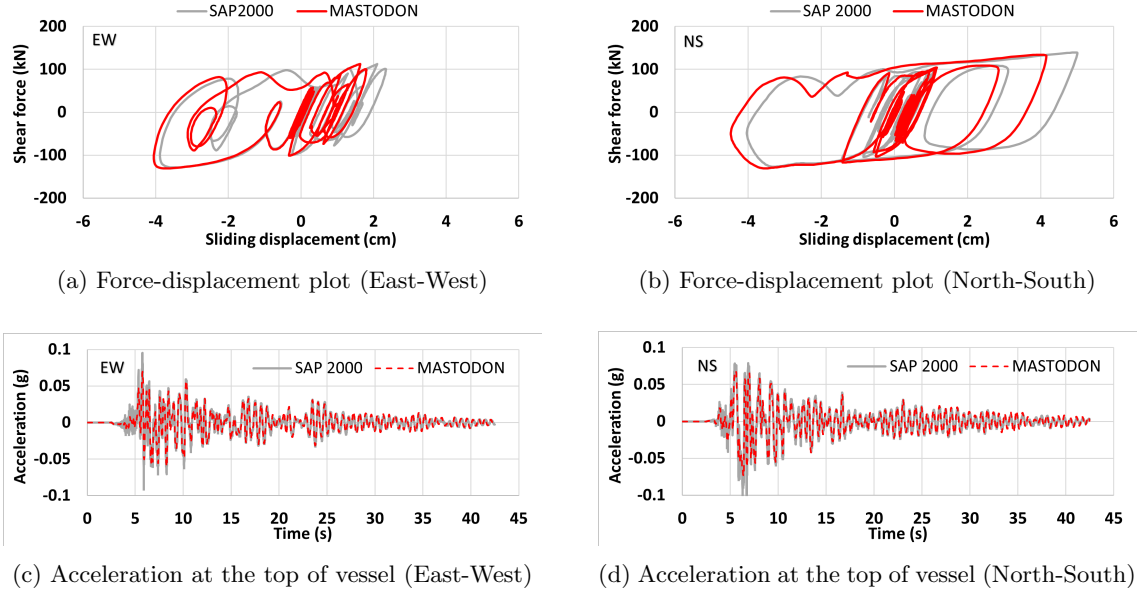


Fig. 13. Comparison of response in isolated (lead-rubber) vessel for fixed base model ID - I

13(a) and 13(b). The peak acceleration response in the vessel along East-West and North-South directions are compared in Figures 13(c) and 13(d). The plots show that results from SAP 2000 and MASTODON match well with each other. The single friction pendulum and lead-rubber bearings also have similar behavior in terms of yield force of about 110 kN and bearing displacement between 40 mm and 50 mm since they are assigned similar properties in shear.

Finally, results from soil-structure interaction models using friction pendulum isolators in MASTODON and SAP 2000 are compared. Figure 14 presents spectral acceleration at the top of the isolated vessel of Model ID - I for Pilgrim site and subjected to seismic excitation corresponding to Loma Prieta earthquake. The rock outcrop motion is also plot for reference. The analysis in SAP 2000 is based on multi-support excitation of the isolated vessel and the four isolators where 3-component displacement time-series at the bottom node of each isolator is obtained from an analysis in MASTODON and is then used as input motion in SAP 2000.

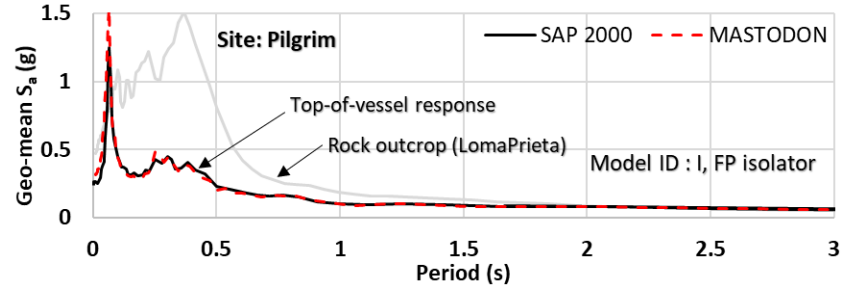


Fig. 14. Comparison of acceleration response spectra in an isolated vessel from soil-structure interaction analyses in MASTODON and multi-support excitation in SAP 2000.

### Trajectory of bearings during different seismic excitations

Trajectories of the bearings during different seismic events are plot in Figure 15 for the fixed base model. Circles with radius equal to the design displacement are drawn for reference. The plots are obtained from analysis using RPV Model ID - I. It is found that the trajectory of the bearing is not affected by the fundamental frequency of the vessel and remains identical for models ID - II, III and IV. Displacement of the bearing does not necessarily correlate with any measure of earthquake intensity given the random nature of ground motions in terms of frequency content. The largest bearing displacement occurs for the Manjil ground motion which has the largest  $S_{D1}$  (spectral acceleration at 1s period) as tabulated in Table VI. For all the ground motions considered, the displacement of the isolator is within the design displacement of the bearing.

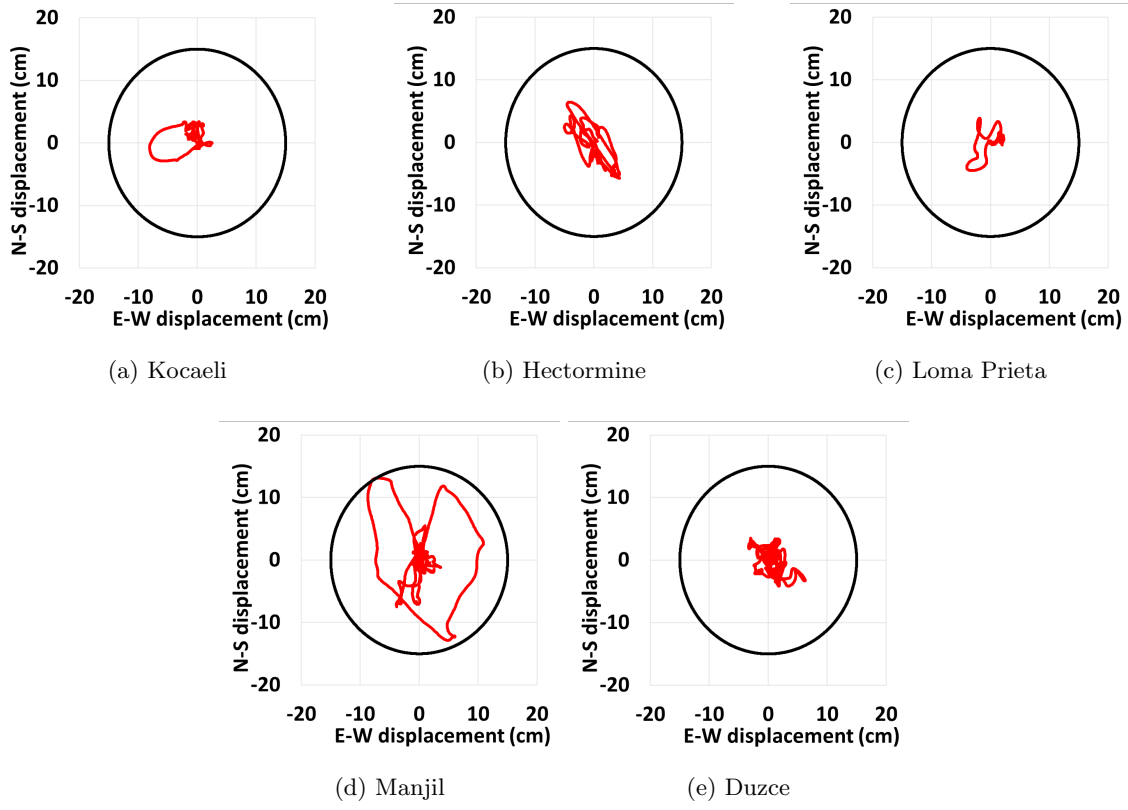


Fig. 15. Trajectories of bearings for different ground motions from fixed base analyses

### Results for analyses conducted with a fixed base

Table VII summarizes the peak acceleration response in the RPV conducted with a fixed base boundary condition. The model IDs are as described in Table I and analyses conducted with lead-rubber isolators are labeled as LR. The peak geo-mean acceleration at the bottom of the isolator is the same as that in the rock outcrop motion, listed in column (iv). Peak geo-mean acceleration at the top of one of the isolators is listed in column (v). The horizontal acceleration response in all four isolators is almost identical. Rotational acceleration at the isolation interface is extracted at the node intersecting the link beams and the vertical beam and listed in column (vi). In the RPV, the peak acceleration occurs farthest from its support location which is at the top of the vessel, listed in column (vii). The difference between the peak acceleration at the top-of-vessel and the top-of-isolator is tabulated in column (viii). Note that the horizontal acceleration at the top of RPV due to rotation of the isolation interface can be obtained by multiplying ( $\ddot{\theta}$ ) with the unsupported height of the vessel,  $(1 - \phi)H$ . It is found that the difference between peak

acceleration at the top-of-vessel and the top-of-isolator can largely be attributed to the effect of the rotational acceleration. A separate analysis is conducted without using seismic isolators and the peak acceleration in the RPV is reported in column (ix). The reduction in peak acceleration due to seismic isolation as defined in Eq. 9 is presented in column (x) of the table.

TABLE VII  
Peak horizontal acceleration in vessel with fixed base model

| SN  | Input motion | Model ID | Peak geo-mean acceleration (g) |      |                         |                 |            |                     | $\eta_a$ (%) |
|-----|--------------|----------|--------------------------------|------|-------------------------|-----------------|------------|---------------------|--------------|
|     |              |          | Isolator                       |      | Rot. acc. ( $rad/s^2$ ) | Isolated vessel |            | Non-isolated vessel |              |
|     |              |          | Bottom                         | Top  |                         | Total           | Difference |                     |              |
| (i) | (ii)         | (iii)    | (iv)                           | (v)  | (vi)                    | (vii)           | (vii)-(v)  | (ix)                | (x)          |
| 1   | Kocaeli      | I        | 0.19                           | 0.08 | 2.2e-5                  | 0.08            | 0.00       | 0.22                | 64           |
| 2   |              | I, LR    | 0.19                           | 0.08 | 1.5e-3                  | 0.08            | 0.00       | 0.22                | 66           |
| 3   |              | II       | 0.19                           | 0.10 | 1.2e-2                  | 0.15            | 0.05       | 0.46                | 66           |
| 4   |              | III      | 0.19                           | 0.14 | 1.4e-2                  | 0.24            | 0.10       | 0.69                | 65           |
| 5   |              | IV       | 0.19                           | 0.17 | 2.1e-2                  | 0.35            | 0.18       | 1.02                | 66           |
| 6   | Hectormine   | I        | 0.30                           | 0.08 | 2.3e-5                  | 0.09            | 0.01       | 0.33                | 74           |
| 7   |              | II       | 0.30                           | 0.09 | 1.2e-2                  | 0.15            | 0.06       | 0.46                | 68           |
| 8   |              | III      | 0.30                           | 0.13 | 1.4e-2                  | 0.25            | 0.12       | 1.42                | 82           |
| 9   |              | IV       | 0.30                           | 0.15 | 2.0e-2                  | 0.33            | 0.18       | 1.90                | 82           |
| 10  | Loma Prieta  | I        | 0.45                           | 0.08 | 2.0e-5                  | 0.09            | 0.01       | 0.70                | 88           |
| 11  |              | I, LR    | 0.45                           | 0.07 | 4.0e-3                  | 0.07            | 0.00       | 0.70                | 90           |
| 12  |              | II       | 0.45                           | 0.09 | 1.1e-2                  | 0.14            | 0.05       | 1.17                | 88           |
| 13  |              | III      | 0.45                           | 0.15 | 1.6e-2                  | 0.30            | 0.15       | 1.76                | 83           |
| 14  |              | IV       | 0.45                           | 0.14 | 1.7e-2                  | 0.27            | 0.13       | 2.13                | 87           |
| 15  | Manjil       | I        | 0.51                           | 0.11 | 3.9e-5                  | 0.12            | 0.01       | 0.61                | 80           |
| 16  |              | II       | 0.51                           | 0.12 | 1.6e-2                  | 0.18            | 0.06       | 2.35                | 92           |
| 17  |              | III      | 0.51                           | 0.18 | 2.3e-2                  | 0.38            | 0.20       | 4.61                | 92           |
| 18  |              | IV       | 0.51                           | 0.22 | 3.2e-2                  | 0.44            | 0.22       | 2.98                | 85           |
| 19  | Duzce        | I        | 0.88                           | 0.10 | 6.3e-5                  | 0.11            | 0.01       | 1.21                | 91           |
| 20  |              | II       | 0.88                           | 0.13 | 2.1e-2                  | 0.22            | 0.09       | 1.33                | 83           |
| 21  |              | III      | 0.88                           | 0.17 | 2.5e-2                  | 0.38            | 0.21       | 6.51                | 94           |
| 22  |              | IV       | 0.88                           | 0.21 | 1.7e-2                  | 0.45            | 0.24       | 6.26                | 93           |

The peak acceleration in the vessel ( $a_{peak}$  as defined in Eq. 8) corresponding to fundamental frequency of RPV is presented in Figure 16. The peak acceleration in RPV Model ID - I (fundamental frequency about 24 Hz) is around 0.1g. For RPV Model ID - III and IV, it increases to a value between 0.25g to 0.45g depending upon the frequency content of the input motion. The plot indicates that the peak acceleration in the vessel decreases with increase in fundamental frequency of the vessel for all the ground motions considered. There is record-to-record variability

which is more evident at lower frequencies of the vessel. The RPV Model ID - I behaves almost like a rigid component due to which the response in the vessel is similar to that of the top of the isolator. With decrease in fundamental frequency of RPV, the difference between the top-of-vessel and top-of-isolator acceleration grows because of contribution from higher modes of the isolated system.

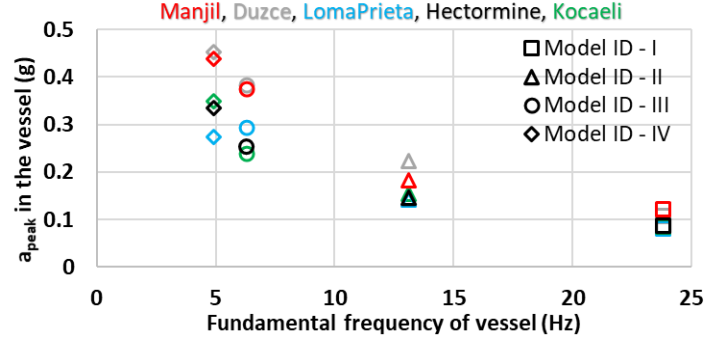


Fig. 16. Peak acceleration in vessel for different fundamental frequency of vessel from analysis with fixed base

Table VIII summarizes the peak vertical downward acceleration on the isolators for the analyses conducted with a fixed base. Friction pendulum (FP) isolators are vertically stiff and do not amplify the motion in the vertical direction. We note that with FP isolators, peak vertical acceleration resulting from a particular ground motion is independent of the RPV model used in the analysis. On the other hand, lead rubber (LR) isolators have limited stiffness in vertical direction which amplifies vertical acceleration as indicated in Table VIII. Lead rubber isolators are used only for select cases of RPV Model ID-I subjected to Kocaeli and Loma Prieta ground motions since further analyses would not result in any new finding.

Figure 17 presents the minimum axial compression in the isolators obtained from time-history analysis compared to a references value. The reference value is computed using peak vertical downward acceleration from Table VIII treating the vessel and the isolator as rigid masses as:

$$P_{min} = W_{iso} \left( 1 - \frac{a_v}{g} \right) \quad (10)$$

where,  $W_{iso}$  is the static force on each isolator equal to one-fourth the weight of the vessel,  $a_v$  is vertical acceleration at the top-of-isolator and  $g$  is acceleration due to gravity. Note that under

the assumption that both the isolator and the vessel are rigid masses, if the bottom and top of the isolator accelerate downward with  $g$ , then the internal force in the isolator reduces to zero. For RPV Model ID - I,  $P_{min}$  obtained from numerical analysis and from Eq. 10 are in good agreement. This is because the RPV Model ID - I is supported such that its center of mass aligns with the isolation interface and it also behaves like a rigid component. The tendency of lead-rubber bearing to develop tensile forces or friction pendulum bearing to uplift is stimulated by aligning the center of mass of RPV away from its support location. Despite being supported at quarter height, RPV Model IDs - III and IV have unsupported heights of 20.6m compared to 13.7m for RPV Model ID - II. Taller vessels therefore produce larger overturning moment at the isolation interface which reduces the minimum axial force ( $P_{min}$ ) in the isolators for RPV Model IDs - III and IV compared to RPV Model ID-II as indicated in Figure 17.

TABLE VIII  
Peak vertical acceleration in fixed base model

| SN | Input motion | Model ID | Isolator | Peak vertical acceleration (g) <sup>†</sup> |                 |
|----|--------------|----------|----------|---|-----------------|
|    |              |          |          | Bottom of isolator                          | Top of isolator |
| 1  | Kocaeli      | All      | FP       | 0.12  | 0.12            |
| 2  |              | I        | LR       | 0.12  | 0.34            |
| 3  | Hectormine   | All      | FP       | 0.15  | 0.15            |
| 4  | Loma Prieta  | All      | FP       | 0.21  | 0.21            |
| 5  |              | I        | LR       | 0.21  | 0.30            |
| 6  | Manjil       | All      | FP       | 0.48  | 0.48            |
| 7  | Duzce        | All      | FP       | 0.32  | 0.32            |

<sup>†</sup> Peak vertical acceleration in downward direction

SS: Changed Table VIII as discussed. Why include the result from LR isolators in this Table if it is not included in the Figure 17? Besides, I don't think running two cases for LR is sufficient.

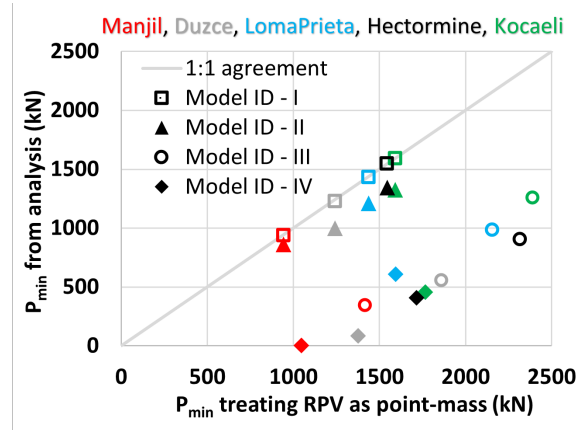


Fig. 17. Minimum axial compression ( $P_{min}$ ) in isolator from analysis with fixed base

### Trajectory of bearings for different sites

Trajectories of a typical bearing for different sites subjected to the Loma Prieta ground motion are plot in Figure 18. The circle of radius equal to the design displacement is drawn for reference. The plots are obtained for RPV Model ID - I using friction pendulum isolator. In this study, design displacement of isolators is based on spectral acceleration at 1-second period of 0.4g. The bearing displacement increases in presence of soil compared to fixed base due to site amplification at frequency corresponding to the fundamental mode of the isolator. For all sites subjected to Loma Prieta ground motion, the displacement of the isolator is within the design displacement of the bearing. For beyond-design events, a fail-safe mechanism to limit bearing displacement must also be designed but it is only engaged when the design displacement is exceeded.

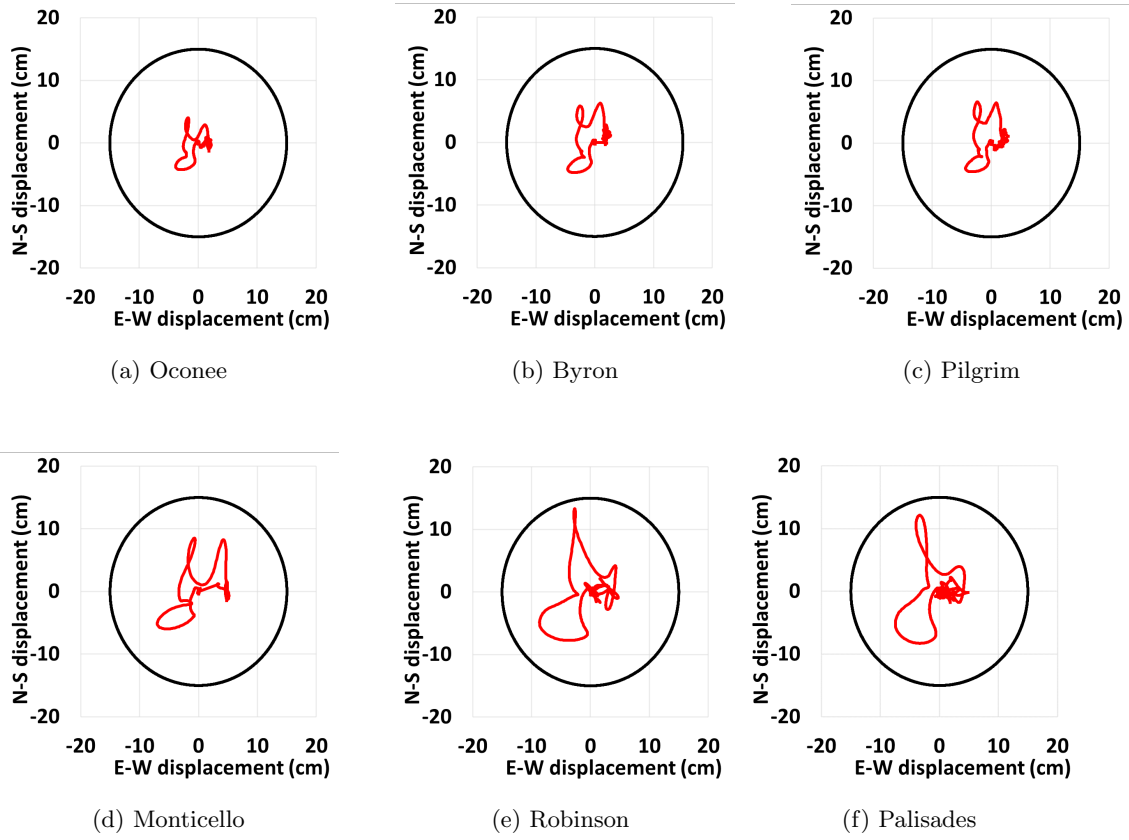


Fig. 18. Trajectory of bearings for different sites during Loma Prieta seismic event.

### Results from analyses conducted using models with soil domain (SSI models)

Table IX summarizes the peak horizontal acceleration in the vessel from numerical analyses conducted using models including the soil domain. The flexibility of soil causes amplification in accelerations depending upon the site and input motion. From Table IX, it is observed that the bottom-of-isolator acceleration resulting from a particular ground motion does not depend upon RPV model but largely depends on site amplification. For instance, irrespective of RPV model, the peak bottom-of-isolator acceleration is around 0.3g for Pilgrim site subjected to Kocaeli ground motion and 0.9g for the same site subjected to Loma Prieta ground motion. Subjected to Loma Prieta ground motion, peak bottom-of-isolator acceleration ranges from 0.7g to 0.9g depending upon the site. At the top of the isolator, site-specific differences in peak acceleration reduce but it is affected noticeably by RPV model. Rotational acceleration at the isolation interface is found to be an order of magnitude greater than that in the case of hard rock or fixed base conditions. The



difference between peak acceleration in RPV Model ID - I and top-of-isolator for different sites can be attributed to the effect of the rotational acceleration ( $\ddot{\theta}$ ).

For each case, a separate analysis is conducted without seismic isolators and the peak acceleration in the RPV is tabulated in column (ix). Finally, reduction in peak acceleration due to seismic isolation ( $\eta_a$ ) is provided in column (x) of Table IX. Analyses are conducted for all sites considering RPV Model ID - I supported on friction pendulum isolators and subjected to Loma Prieta ground motion. Only select analyses are conducted for other RPV models, isolator types and ground motions since they didn't produce any new observation.

Comment on the “missing” rows in the Table. Again, what observations and insights do you gain from this Table? SS: Added more description.

TABLE IX  
Peak horizontal acceleration in vessel from analysis with SSI model

| SN  | Input motion | Site       | Model ID | Peak geo-mean acceleration (g) |          |       |                         |                 |            |                     | $\eta_a$ (%) |
|-----|--------------|------------|----------|--------------------------------|----------|-------|-------------------------|-----------------|------------|---------------------|--------------|
|     |              |            |          | Rock outcrop                   | Isolator |       | Rot. acc. ( $rad/s^2$ ) | Isolated vessel |            | Non-isolated vessel |              |
|     |              |            |          |                                | Bottom   | Top   |                         | Total           | Difference |                     |              |
| (i) | (ii)         | (iii)      | (iv)     | (v)                            | (vi)     | (vii) | (viii)                  | (ix)            | (ix)-(vii) | (xi)                | (xii)        |
| 1   | Kocaeli      | Pilgrim    | I        | 0.19                           | 0.32     | 0.09  | 0.06                    | 0.13            | 0.04       | 0.53                | 74.8         |
| 2   |              |            | I, LR    | 0.19                           | 0.31     | 0.08  | 0.06                    | 0.12            | 0.04       | 0.53                | 76.7         |
| 3   |              |            | II       | 0.19                           | 0.32     | 0.19  | 0.12                    | 0.33            | 0.14       | 1.12                | 70.1         |
| 4   |              |            | III      | 0.19                           | 0.31     | 0.15  | 0.06                    | 0.33            | 0.18       | 1.92                | 83.0         |
| 5   | Loma Prieta  | Pilgrim    | I        | 0.45                           | 0.90     | 0.11  | 0.19                    | 0.31            | 0.20       | 1.38                | 77.7         |
| 6   |              |            | I, LR    | 0.45                           | 0.90     | 0.08  | 0.21                    | 0.24            | 0.16       | 1.38                | 82.4         |
| 7   |              |            | II       | 0.45                           | 0.91     | 0.25  | 0.19                    | 0.42            | 0.17       | 3.05                | 86.3         |
| 8   |              |            | III      | 0.45                           | 0.89     | 0.30  | 0.14                    | 0.57            | 0.27       | 4.15                | 86.2         |
| 9   | Kocaeli      | Palisades  | I        | 0.19                           | 0.43     | 0.10  | 0.26                    | 0.33            | 0.23       | 0.76                | 56.7         |
| 10  |              |            | II       | 0.19                           | 0.43     | 0.19  | 0.25                    | 0.37            | 0.18       | 0.99                | 62.9         |
| 11  | Loma Prieta  | Palisades  | I        | 0.45                           | 0.70     | 0.11  | 0.48                    | 0.57            | 0.46       | 1.21                | 53.0         |
| 12  |              |            | II       | 0.45                           | 0.70     | 0.28  | 0.43                    | 0.61            | 0.33       | 1.45                | 57.8         |
| 13  | Loma Prieta  | Byron      | I        | 0.45                           | 0.72     | 0.09  | 0.03                    | 0.11            | 0.20       | 0.96                | 88.8         |
| 14  | Loma Prieta  | Monticello | I        | 0.45                           | 0.92     | 0.12  | 0.47                    | 0.68            | 0.56       | 1.41                | 51.9         |
| 15  | Loma Prieta  | Robinson   | I        | 0.45                           | 0.74     | 0.13  | 0.39                    | 0.56            | 0.43       | 1.28                | 56.5         |

Figure 19 plots the peak acceleration in the seismically isolated RPV Model ID - I against the shear wave velocity of site. RPV Model ID - I is particularly considered for its near-rigid behavior not to downplay the deformation in the vessel but to decouple the effect of soil flexibility. Ground motion from Loma Prieta earthquake is used for the analyses. It is observed that peak acceleration in the RPV which is influenced by the rotational acceleration at the isolation interface as given in Eq. 1 increases with decrease in shear wave velocity of the sites. It must be noted

that such increase is due to larger rotational acceleration in softer sites and not resulting from site amplification since the peak acceleration at the top of the isolator is similar irrespective of site (ranging from 0.09g to 0.13g for RPV Model ID-I, see Table IX). Figure 19 also shows that the peak acceleration in the isolated vessel increases sharply (more than five times) in softer sites ( $v_{s30}$  below 500m/s) compared to fixed base. This highlights the significance of considering soil-structure interaction for component isolation.

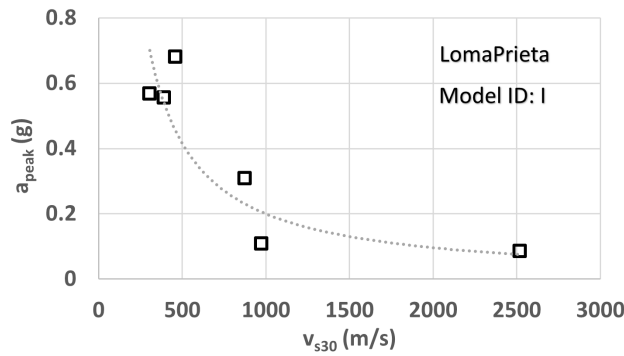


Fig. 19. Peak horizontal acceleration in vessel for different sites

Table X summarizes the minimum axial load on the isolators for the analyses conducted with explicit modeling of the soil domain. The minimum axial compression on the isolators is obtained from time-history analysis. For reference, it is also calculated assuming rigid base and treating RPV as a point-mass, as per Eq. 10. The calculated  $P_{min}$  differs from that obtained from analysis due to foundation rocking induced by the interaction between soil and the embedded sub-structure.

Figure 20 plots the minimum axial compression in friction pendulum seismic isolators during the seismic excitation by Loma Prieta earthquake using RPV Model ID - I. The plot reflects a trend showing that the isolators are more vulnerable to uplift when they are used at sites with lower shear wave velocity. For relatively softer sites ( $v_{s30} < 500$  m/s) such as Monticello and Robinson, one of the isolators uplifts during the seismic event although the peak vertical acceleration is only around 0.4g. This is not desirable due to possibility of impact load on re-engagement of the isolator which is not captured in SAP 2000 or MASTODON models.

TABLE X  
Minimum axial compression in isolators with SSI model

| SN  | Input motion | Site       | Model ID | Peak vertical acceleration (g) <sup>†</sup> |                 | Static load (kN) | $P_{min}$ (kN)   |               |
|-----|--------------|------------|----------|---|-----------------|------------------|--|---------------|
|     |              |            |          | Bottom of isolator                          | Top of isolator |                  | Calculated for rigid base and treating RPV as point-mass (vii) $\times [1 - (vi)]$ | From analysis |
| (i) | (ii)         | (iii)      | (iv)     | (v)   | (vi)            | (vii)            | (viii)   | (ix)          |
| 1   | Kocaeli      | Pilgrim    | I        | 0.35  | 0.35            | 1815             | 1179   | 943           |
| 2   |              |            | I, LR    | 0.24  | 0.68            | 1815             | 578  | 498           |
| 3   |              |            | II       | 0.35  | 0.35            | 1815             | 1170   | 649           |
| 4   |              |            | III      | 0.36  | 0.36            | 2722             | 1735   | 641           |
| 5   | Loma Prieta  | Pilgrim    | I        | 0.46  | 0.46            | 1815             | 974  | 663           |
| 6   |              |            | I, LR    | 0.37  | 0.49            | 1815             | 921  | 601           |
| 7   |              |            | II       | 0.48  | 0.48            | 1815             | 939  | 222           |
| 8   |              |            | III      | 0.50  | 0.50            | 2722             | 1348   | 0             |
| 9   | Kocaeli      | Palisades  | I        | 0.25  | 0.25            | 1815             | 1357   | 947           |
| 10  |              |            | II       | 0.25  | 0.25            | 1815             | 1352   | 645           |
| 11  | Loma Prieta  | Palisades  | I        | 0.33  | 0.33            | 1815             | 1219   | 329           |
| 12  |              |            | II       | 0.33  | 0.33            | 1815             | 1219   | 338           |
| 13  | Loma Prieta  | Byron      | I        | 0.33  | 0.33            | 1815             | 1214   | 1028          |
| 14  | Loma Prieta  | Monticello | I        | 0.40  | 0.40            | 1815             | 1090   | 0             |
| 15  | Loma Prieta  | Robinson   | I        | 0.43  | 0.43            | 1815             | 1041   | 0             |

<sup>†</sup> Peak vertical acceleration in downward direction

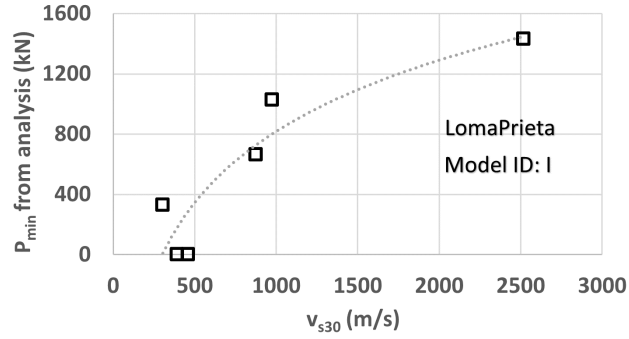


Fig. 20. Minimum axial compression ( $P_{min}$ ) in isolator from analysis for different sites, using 1989 Loma Prieta record on model ID: I

### Comparison between isolated and non-isolated vessel

Figure 21 plots the comparison of geo-mean spectral acceleration at three locations in the model: the bottom-of-isolator, the top-of-isolator and the top-of-vessel from analysis on RPV Model ID - I subjected to the Loma Prieta input motion. One of the four isolators is arbitrarily selected for the plot because there is little variation in the spectral acceleration response of different isolators. Peak spectral acceleration in the RPV with and without the use of seismic isolators is also presented in Figure 21.

For fixed base boundary condition, the spectral acceleration is identical at the top of isolator and the top of vessel. An amplification is observed at around the fundamental frequency of the vessel (23.8 Hz) when the RPV is not seismically isolated. For Pilgrim site, the spectral acceleration at the top of isolator and the top of vessel exhibit maximum difference at a particular frequency of about 16 Hz for single friction pendulum bearings and about 6 Hz for lead-rubber bearings. Those are the frequencies corresponding to the rotational acceleration at the isolation interface. The rotational acceleration has a dominant frequency of 16 Hz when the RPV is not seismically isolated. The dominant frequency is unchanged even after installing friction pendulum isolators because of their high rotational stiffness. But, installing lead-rubber bearings, which are flexible, reduces the dominant frequency to about 6 Hz.

For both friction pendulum and lead-rubber bearings, the peak acceleration in the vessel (zero period spectral acceleration) is about 3 times higher (from around 0.1g to 0.3g) than that at the top of the isolators. Nevertheless, compared to the non-isolated vessel, seismic isolation reduces the peak acceleration in the vessel by more than 50%. This reduction of peak acceleration in the RPV is plot against rock outcrop PGA in Figure 22. The reduction of peak acceleration in the RPV is not dependent on the fundamental frequency of the vessel. It ranges from 70% to about 85% for rock outcrop PGA of 0.2g to 0.9g for fixed base condition. The results from different sites are also plot for the Loma Prieta input motion ( $PGA = 0.45g$ ). For sites such as Monticello, Palisades and Robinson which have relatively lower  $v_{s30}$ , the reduction of peak acceleration from seismic isolation is also comparatively lower at around 50%. For stiffer sites such as Byron and Pilgrim, the reduction is around 80%.

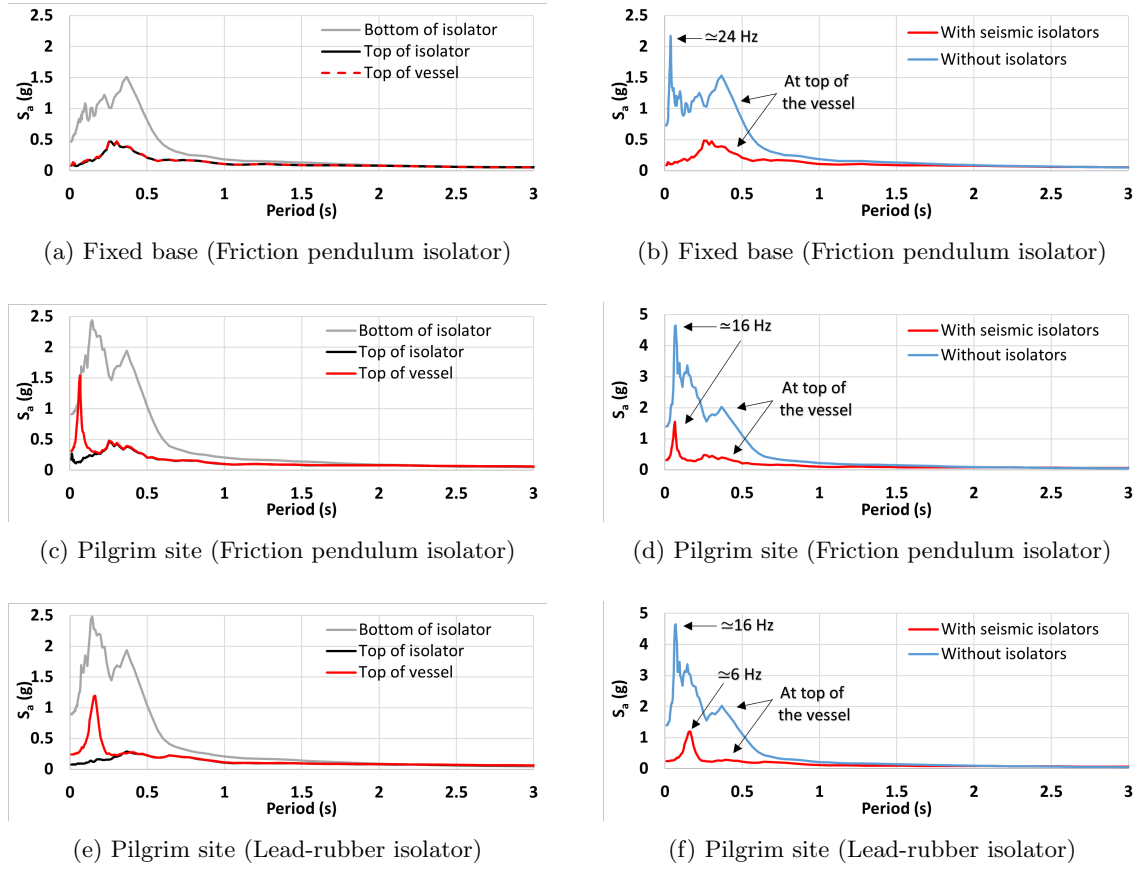


Fig. 21. Comparison of spectral acceleration response for different cases using RPV Model ID - I and Loma Prieta input motion

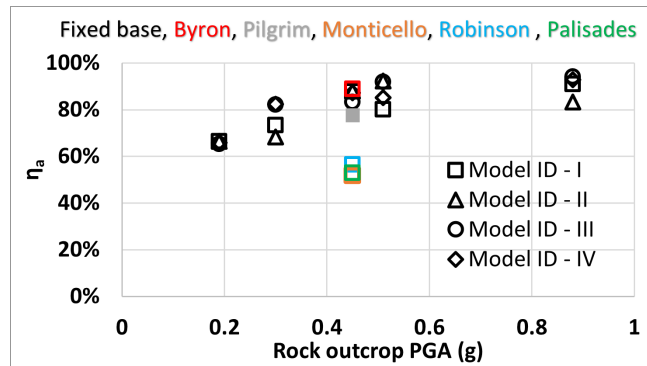


Fig. 22. Reduction of peak acceleration in vessel from seismic isolation **Model ID 1V ? Oconee?**  
**Symbol colors for different ground motions? Is this data from Table X ?**  
**SS: Model IV added, Oconee same as Fixed base, Ground motion distinguished by rock outcrop PGA, data from Table IX**

## VIII. CONCLUSIONS

From the numerical analysis on the conceptual component isolation model, the following conclusions can be drawn:

1. The fixed base boundary condition is a good approximation for hard rock sites such as Oconee which is shallow (20.4m depth) and has a shear wave velocity of 2520 m/s. This is in agreement with ASCE 4-16 [37] which allows fixed base analysis for sites with average shear wave velocity above 2400 m/s.
2. The optimum location to support a component for seismic isolation is on a plane passing through its center of mass. Even when the component is supported at its center of mass, the rotation of sub-structure can cause rotational acceleration at the isolation interface which translates into horizontal acceleration in the vessel. Tall vessels or components are particularly vulnerable to this phenomenon.
3. The rotational acceleration at the isolation interface is influenced by shear wave velocity of soil. For the configuration of sub-structure and isolators considered in this study, the horizontal acceleration in the vessel caused by rotational acceleration at the isolation interface increases with decrease in shear wave velocity of soil. The increase in acceleration demand and therefore lateral forces in the vessel resulting from soil-structure interaction is significant and should not be neglected particularly for sites with soft soil and even for stiffer soil with average shear wave velocity of around 900 m/s.
4. Isolators can develop tensile forces or uplift even when the input motion has a vertical acceleration lower than 1g. This happens because the overturning moment at the isolation interface decreases the axial compression in some isolators.
5. Horizontal displacement in isolators is affected by amplification caused by flexibility of soil at the fundamental period of the isolated system. In cases where design displacement of the bearings is exceeded, a fail-safe mechanism should exist. This justifies the requirement of having a physical stop for an isolated system to limit the bearing displacement that may cause safety issues in safety-critical components.

6. Spectral acceleration in the isolated vessel is significantly (more than 50%) lower than in its non-isolated counterpart across all periods except the long-period range ( $> 2$  seconds). In that sense, component isolation using conventional seismic isolators such as friction pendulum and lead-rubber bearings is beneficial unless unexpected forces may occur due to cavitation in rubber or impact after uplifting of friction pendulum bearing.

## REFERENCES

- [1] A. S. WHITTAKER, P. SOLLOGOUB, and M. K. KIM, “Seismic isolation of nuclear power plants: Past, present and future,” *Nuclear Engineering and Design*, **338**, 290 (2018).
- [2] Y. TSUBOI, K. ARIE, N. UEDA, T. GRENCI, and A. YACOUT, “Design of the 4S Reactor,” *Nuclear Technology*, **178**, 2, 201 (2012).
- [3] M. FORNI, A. POGGIANTI, F. BIANCHI, G. FORASASSI, R. LO FRANO, G. PUGLIESE, F. PEROTTI, L. CORRADI DELL’ACQUA, M. DOMANESCHI, M. D. CARELLI ET AL., “Seismic isolation of the IRIS nuclear plant,” *ASME Pressure Vessels and Piping Conference*, vol. 43710, 289–296 (2009).
- [4] A. DUSI ET AL., “Seismic isolation of nuclear power plants,” *15th World Conference on Earthquake Engineering* (2012).
- [5] F. TAJIRIAN, E. GLUEKLER, W. CHEN, and J. KELLY, “Qualification of high damping seismic isolation bearings for the ALMR,” (1992).
- [6] A. KAMMERER, A. WHITTAKER, and M. CONSTANTINOU, *Technical considerations for seismic isolation of nuclear facilities*, NUREG/CR-7253, United States Nuclear Regulatory Commission, Washington, DC (2019).
- [7] B. STOJADINOVIC, “Technical considerations for seismic isolation of nuclear facility structures,” *UC Berkeley* (2011).
- [8] M. C. CONSTANTINOU, A. WHITTAKER, Y. KALPAKIDIS, D. FENZ, and G. P. WARN, “Performance of seismic isolation hardware under service and seismic loading,” *Technical Rep. No. MCEER-07*, **12** (2007).
- [9] F. NAEIM and J. M. KELLY, *Design of seismic isolated structures: from theory to practice*, John Wiley & Sons (1999).
- [10] I. G. BUCKLE and R. L. MAYES, “Seismic isolation: history, application, and performance—a world view,” *Earthquake spectra*, **6**, 2, 161 (1990).



- [11] I. G. BUCKLE, “New Zealand seismic base isolation concepts and their application to nuclear engineering,” *Nuclear Engineering and Design*, **84**, 3, 313 (1985).
- [12] M. KUMAR, A. S. WHITTAKER, and M. C. CONSTANTINOU, “Extreme earthquake response of nuclear power plants isolated using sliding bearings,” *Nuclear Engineering and Design*, **316**, 9 (2017).
- [13] U. N. R. COMMISSION ET AL., *Regulatory guide 1.208: a performance-based approach to define the site-specific earthquake ground motion*, US Nuclear Regulatory Commission, Office of Nuclear Regulatory Research (2007).
- [14] C. BOLISSETTI, C. YU, J. COLEMAN, A. WHITTAKER, and B. KOSBAB, “Characterizing the benefits of seismic isolation for nuclear structures: a framework for risk-based decision making,” , Idaho National Lab.(INL), Idaho Falls, ID (United States) (2016).
- [15] A. KAMMERER, A. WHITTAKER, and J. COLEMAN, *Regulatory gaps and challenges for licensing advanced reactors using seismic isolation*, INL/EXT-15-36945, Idaho National Laboratory, Idaho Falls, Idaho (2016).
- [16] Y.-S. CHOON, “Seismic Isolation Studies and Applications for Nuclear Facilities,” *Proceedings of the Korean Nuclear Society Conference*, 436–437, Korean Nuclear Society (2005).
- [17] K. EBISAWA, K. ANDO, and K. SHIBATA, “Progress of a research program on seismic base isolation of nuclear components,” *Nuclear Engineering and Design*, **198**, 1-2, 61 (2000).
- [18] K. EBISAWA, K. ANDO, H. KAMEOKA, and K. SHIBATA, “Influence of soil properties on response of seismic base isolation of nuclear equipment,” *Transaction of the 14th International Conference on Structural Mechanics in Reactor Technology (SmiRT 14)* (1997).
- [19] C. A. KIRCHER, G. C. DELFOSSE, C. C. SCHOOF, O. KHEMICI, and H. C. SHAH, *Performance of a 230 KV ATB 7 power circuit breaker mounted on Gapec seismic isolators*, Report No. 79/40, John A. Blume Earthquake Engineering Center, Stanford University (1979).
- [20] D. FORCELLINI, L. FACCHINI, M. BETTI, C. MORANDINI, D. CLYDE, and P. SEGAS, “Seismic protection systems for artifacts: a base isolation proposal for Michelangelo’s David,” *Proceedings of the 14th World Conference on Seismic Isolation, Energy Dissipation and Active Vibration Control of Structures (14WCSI)*. San Diego, California, USA (2015).

- [21] J. YAGHOUBIAN, “Isolating building contents from earthquake induced floor motions,” *Earthquake spectra*, **7**, 1, 127 (1991).
- [22] M. LOWRY, B. FARRAR, D. ARMENDARIZ, and J. PODANY, “Protecting collections in the J. Paul Getty Museum from earthquake damage,” *WAAC newsletter*, **29**, 3, 16 (2007).
- [23] V. LAMBROU and M. C. CONSTANTINOU, *Study of seismic isolation systems for computer floors*, National Center for Earthquake Engineering Research (1994).
- [24] M. HAMIDI and M. EL NAGGAR, “On the performance of SCF in seismic isolation of the interior equipment of buildings,” *Earthquake engineering & structural dynamics*, **36**, 11, 1581 (2007).
- [25] G. A. AUAD and J. L. ALMAZÁN, “Non linear vertical-rocking isolation system: Application to legged wine storage tanks,” *Engineering Structures*, **152**, 790 (2017).
- [26] S. I. REYES and J. L. ALMAZÁN, “A novel device for a vertical rocking isolation system with uplift allowed for industrial equipment and structures,” *Engineering Structures*, **214**, 110595 (2020).
- [27] M. F. VASSILIOU and N. MAKRIS, “Analysis of the rocking response of rigid blocks standing free on a seismically isolated base,” *Earthquake Engineering & Structural Dynamics*, **41**, 2, 177 (2012).
- [28] P. ROUSSIS and M. CONSTANTINOU, “Experimental and analytical study of seismically isolated structures with uplift restraint,” *Proc., 13th World Conf. on Earthquake Engineering* (2004).
- [29] P. C. ROUSSIS and M. C. CONSTANTINOU, *Experimental and analytical studies of structures seismically isolated with an uplift-restraint isolation system*, 1, Multidisciplinary Center for Earthquake Engineering Research (2005).
- [30] M. NOVAK and P. HENDERSON, “Base-isolated buildings with soil-structure interaction,” *Earthquake engineering & structural dynamics*, **18**, 6, 751 (1989).
- [31] N. TONGAONKAR and R. JANGID, “Seismic response of isolated bridges with soil–structure interaction,” *Soil Dynamics and Earthquake Engineering*, **23**, 4, 287 (2003).

- [32] Z. HAIYANG, Y. XU, Z. CHAO, and J. DANDAN, “Shaking table tests for the seismic response of a base-isolated structure with the SSI effect,” *Soil Dynamics and Earthquake Engineering*, **67**, 208 (2014).
- [33] IAEA, “Advanced Reactors Information System,” <https://aris.iaea.org/>.
- [34] D. C. WADE and L. WALTERS, “ARC-100: a sustainable, modular nuclear plant for emerging markets,” *Proceeding of ICAPP*, vol. 10, 13–17 (2010).
- [35] J. COLEMAN, A. SLAUGHTER, S. VEERARAGHAVAN, C. BOLISSETTI, O. A. NUMANOGLU, R. SPEARS, W. HOFFMAN, and E. KURT, “MASTODON theory manual,” , Idaho National Lab.(INL), Idaho Falls, ID (United States) (2017)Code compiled on 19 April 2020.
- [36] CSI, SAP2000, “Analysis Reference Manual,” *Computers and Structures, Inc., Berkeley, California, USA* (2019).
- [37] AMERICAN SOCIETY OF CIVIL ENGINEERS, “Seismic analysis of safety-related nuclear structures and commentary,” American Society of Civil Engineers (2014).
- [38] R. L. KUHLEMEYER and J. LYSMER, “Finite element method accuracy for wave propagation problems,” *Journal of Soil Mechanics & Foundations Div*, **99**, Tech Rpt (1973).
- [39] R. SPEARS, S. VEERARAGHAVAN, and J. COLEMAN, “Nonlinear Modeling of Ground Motions at Lotung LSST Site with Nested Surface Soil Constitutive Model,” *Nuclear Technology*, **205**, 9, 1205 (2019).
- [40] T. J. HUGHES, “Analysis of transient algorithms with particular reference to stability behavior,” *Computational methods for transient analysis, Amsterdam, North-Holland*, 67–155 (1983).
- [41] AMERICAN ASSOCIATION OF STATE HIGHWAY AND TRANSPORTATION OFFICIALS, *Guide specifications for seismic isolation design*, AASHTO (2010).
- [42] M. KUMAR, A. S. WHITTAKER, and M. C. CONSTANTINOU, “Characterizing friction in sliding isolation bearings,” *Earthquake Engineering & Structural Dynamics*, **44**, 9, 1409 (2015).
- [43] V. A. ZAYAS and S. A. MAHIN, *The FPS earthquake resisting system experimental report*, Earthquake Engineering Research Center (1987).

- [44] Y.-K. WEN, “Method for random vibration of hysteretic systems,” *Journal of the engineering mechanics division*, **102**, 2, 249 (1976).
- [45] Y. J. PARK, Y. K. WEN, and A. H. S. ANG, “Random vibrations of hysteretic systems under bi-directional ground motions,” *Earthquake Engineering and Structural Dynamics*, **14**, 4, 543 (1986).
- [46] M. KUMAR, A. WHITTAKER, and M. CONSTANTINOU, *Seismic isolation of nuclear power plants using elastomeric bearings*, United States Nuclear Regulatory Commission, Office of Nuclear Regulatory (2019).
- [47] S. NAGARAJAIAH, A. M. REINHORN, and M. C. CONSTANTINOU, “Nonlinear dynamic analysis of three-dimensional base isolated structures (3D-BASIS),” *Technical Report NCEER-89-0019, National Center for Earthquake Engineering Research, Buffalo, New York* (1989).
- [48] COUNCIL, BUILDING SEISMIC SAFETY, “NEHRP recommended provisions for seismic regulations for new buildings and other structures (FEMA 450),” *Washington, DC* (2003).
- [49] ENTERGY NUCLEAR OPERATIONS, INC., “Seismic hazard and screening report for Palisades Nuclear Plant,” <https://www.nrc.gov/docs/ML1409/ML14090A069.pdf> (2014).
- [50] DUKE ENERGY, “Seismic hazard evaluation for H.B.Robinson Steam Electric Plant, Unit no. 2,” <https://www.nrc.gov/docs/ML1409/ML14099A204.pdf> (2014).
- [51] EXELON GENERATION, “Seismic hazard and screening report for the Byron Generating Station, Units 1 and 2,” <https://www.nrc.gov/docs/ML1409/ML14091A010.pdf> (2014).
- [52] ENERCON, “Seismic hazard and screening report for Oconee Nuclear Station,” <https://www.nrc.gov/docs/ML1409/ML14092A024.pdf> (2014).
- [53] ENTERGY NUCLEAR OPERATIONS, INC., “Seismic hazard and screening report for Pilgrim Nuclear Power Station,” <https://www.nrc.gov/docs/ML1409/ML14092A023.pdf> (2014).
- [54] STEVENSON & ASSOCIATES, “Monticello Nuclear Generating Plant seismic hazard and screening report,” <https://www.nrc.gov/docs/ML1413/ML14136A289.pdf> (2014).

- [55] T. D. ANCHETA, R. B. DARRAGH, J. P. STEWART, E. SEYHAN, W. J. SILVA, B. S.-J. CHIOU, K. E. WOODDELL, R. W. GRAVES, A. R. KOTTKE, D. M. BOORE ET AL., “NGA-West2 database,” *Earthquake Spectra*, **30**, 3, 989 (2014).
- [56] W. D. IWAN, “On a class of models for the yielding behavior of continuous and composite systems,” *Journal of Applied Mechanics* (1967).
- [57] O. A. NUMANOGLU, Y. M. HASHASH, A. CERNA-DIAZ, S. M. OLSON, L. BHAUMIK, C. J. RUTHERFORD, and T. WEAVER, “Nonlinear 3-D modeling of dense sand and the simulation of a soil-structure system under multi-directional loading,” *Geotechnical Frontiers 2017*, 379–388, ASCE.
- [58] D.-Y. CHIANG and J. BECK, “A new class of distributed-element models for cyclic plasticity—I. Theory and application,” *International journal of solids and structures*, **31**, 4, 469 (1994).
- [59] ELECTRIC POWER RESEARCH INSTITUTE (EPRI), “Guidelines for determining design basis ground motions,” (1993).
- [60] M. VUCETIC and R. DOBRY, “Effect of soil plasticity on cyclic response,” *Journal of geotechnical engineering*, **117**, 1, 89 (1991).